Analytical approach to predicting pile self-weight penetration, considering penetration rate effects

Duffy, Kevin; Reale, Cormac; Gavin, Ken

DOI
10.1016/j.oceaneng.2025.121949

Publication date
2025

Document Version
Final published version

Published in
Ocean Engineering

Ocean Engineering 338 (2025) 121949

Contents lists available at ScienceDirect

Ocean Engineering

journal homepage: www.elsevier.com/locate/oceaneng

Research paper

Analytical approach to predicting pile self-weight penetration, considering penetration rate effects

Kevin Duffy [a,*], Cormac Reale [b], Ken Gavin [a,c]

[a] Department of Geoscience & Engineering, TU Delft, the Netherlands
[b] Department of Architecture and Civil Engineering, University of Bath, United Kingdom
[c] InGEO2 Consulting Engineers, Delft, the Netherlands

ARTICLE INFO

Keywords:
Pile run
Self-weight penetration
Monopiles
Static resistance to driving
Cone penetration testing

ABSTRACT

As offshore pile foundations increase in diameter and weight, the risk of uncontrolled and unsafe penetration events (pile run) also increases. Traditional approaches to evaluating this risk rely on static resistance to driving (SRD) formulations, equating the SRD to the effective weight of the pile. However, high penetration speeds during uncontrolled pile penetration can lead to a soil response much different to static conditions, particularly with regards to pore pressure dissipation around the pile. With this in mind, the paper proposes an analytical model for determining when uncontrolled penetration may occur and its extent. The model integrates novel SRD formulations with a penetration rate effect model, both of which are derived from cone penetration test (CPT) measurements. The model's predictions were then benchmarked against industry-standard methods using a database of self-weight penetration events in clays and sands of varying densities and strengths. The predicted self-weight penetrations compared well with field observations across the full range of soil conditions and gave a better performance compared to standard prediction methods. Furthermore, the results emphasise the critical role of soil volumetric behaviour during shearing and future research should clarify the influence of rapid penetration on the pile's shaft and base resistance.

1. Introduction

Offshore structures are often supported on large, open-ended steel piles. Installing these piles is a complex and high-risk operation, especially since the pile and hammer often weigh up to thousands of tonnes. As a result, lifting and installing these components from a heavy-lift vessel requires meticulous planning. One example of an installation is given in Fig. 1: it begins with "stabbing" the pile, where the pile is carefully lowered to the seabed and placed in a pile guide frame. The pile then penetrates under its own weight until there is enough soil resistance to stop the pile's momentum. Once self-weight penetration stops, the hammer is slowly placed on top of the pile, occasionally with a piling template or sleeve to improve load transfer from the hammer to the pile.

From a design perspective, self-weight penetration can help confirm the soil conditions around the pile and with forecasting the remainder of pile installation (Cathie et al., 2024; Shonberg et al., 2017). For suction caissons, accurate self-weight penetration predictions are also needed to forecast the hydraulic conditions and pumps required for suction-assisted installation (Luo et al., 2025; OWA, 2019). Moreover, the mechanisms controlling self-weight penetration also govern the onset of "pile run," in other words, the uncontrolled penetration of a pile during pile driving. Recent incidents of pile run have created serious safety incidents, delays and economic losses because of the damage it can cause to the pile, hammer, crane and other lifting tools—exacerbated by the ever-increasing size of offshore wind turbines and the deeper water depths in which they are installed. New innovations—like internal lifting tools, clamps or passive heave compensators—can help reduce risks to the lifting equipment and vessel. Regardless, prescribing these tools requires a good understanding of the energy in the pile-hammer system, particularly the pile's acceleration and deceleration during uncontrolled penetration.

Yet accurately modelling uncontrolled penetration events is not trivial. Standard wave equation software for driveability assessments give limited insights into the likelihood of uncontrolled pile penetration. While large deformation numerical modelling has been shown to be effective in understanding the mechanisms controlling high-speed penetration (Dyson et al., 2025; Tian et al., 2022), its computational costs become prohibitive over large, spatially variable sites. As an

* Corresponding author.
E-mail address: k.duffy@tudelft.nl (K. Duffy).

https://doi.org/10.1016/j.oceaneng.2025.121949
Received 7 March 2025; Received in revised form 29 May 2025; Accepted 17 June 2025
Available online 23 June 2025

alternative, designers resort to static resistance to driving (SRD) formulations, equating the upward soil resistance to the downward effective weight of the pile. However, considerable uncertainty exists regarding what SRD formulation should be used (Cathie et al., 2024; Shonberg et al., 2017). Recent research and industry collaboration has culminated in an improved CPT-based design method for the medium-term axial resistance of piles, known as the "Unified" design method (Lehane et al., 2020, 2022b)—later extended to an SRD method in sand (Lehane et al., 2022a). However, the applicability of this method to more dynamic uncontrolled penetration events is not yet clear.

This paper presents an analytical model based on the principle of energy conservation: equating the kinetic energy of the penetrating pile to its potential energy whilst accounting for the pile weight, soil resistance and hydrodynamic forces. To evaluate the model at an elemental level and remove the influence of driving-induced stress changes on the pile, a database of self-weight penetration records was compiled, all in a variety of soft to stiff clays and loose to very dense sands. The analysis highlights specific components of the SRD formulations, as well as other aspects that can affect the likelihood and extent of self-weight penetration.

2. Analytical model

The analytical approach (Fig. 2) is based on the conservation of energy, equating the kinetic energy of the moving pile to the potential energy across a depth increment i, considering the different forces acting on the pile during penetration (Fig. 3):

$$\frac{1}{2}\left(m_p + m_h\right)\left(v_{i+1}{}^2 - v_i^2\right) = \left(W_p + W_h - \left(F_s + F_b\right) - F_{drag} - F_{buoy}\right)\left(z_{b,i+1} - z_{b,i}\right) \quad \text{Equation 1}$$

where m_p is the mass of the pile, m_h is the mass of the hammer (if applicable), v is the velocity of the pile, W_p is the weight of the pile, W_h is the weight of the hammer, F_s is the shaft resistance, F_b is the base resistance (including both the annular resistance F_{ann} and plug resistance F_{plug}), F_{drag} is the inertial drag force, F_{buoy} is the buoyant weight of displaced soil as well as that acting on the pile and hammer (if submerged) and z_b is the elevation of the pile base.

Several authors have considered this approach for assessing pile run (Sun et al., 2016, 2022; Thijssen and Roelen, 2024), torpedo anchors (O'Loughlin et al., 2013) and free-fall penetrometers (Albatal et al., 2020; Chow et al., 2023). The model in this paper presents several adjustments to these models, primarily with respect to the static resistance to driving formulations (F_s and F_b) and the influence of penetration rate on the pile resistance.

2.1. Static resistance to driving (SRD)

The static resistance to driving represents the short-term axial capacity in terms of the pile's annular resistance F_{ann}, plug resistance F_{plug} and shaft resistance F_s. To predict each resistance component, SRD methods often link the penetration resistance with in-situ tests such as the CPT and there are a range of different SRD methods (Alm and Hamre, 2001; Buckley et al., 2023; DNV, 2019; Jones et al., 2020; Lehane et al., 2022a; Maynard et al., 2019; Schneider and Harmon, 2010; Semple and Gemeinhardt, 1981; Stergiou et al., 2023; Stevens et al., 1982; Toolan and Fox, 1977), each calibrated based on installation databases and adjusted to accommodate for new insights into pile behaviour. To consider an SRD method for assessing self-weight penetration and pile run, each resistance component is explored in the following sections.

2.1.1. Annular resistance in clay and sand

During pile driving, the stress acting on the annulus q_{ann} is often modelled at a base displacement of 2.5 mm, otherwise known as the "toe quake." SRD methods, like that by Alm and Hamre (2001) or Schneider and Harmon (2010), often recommend a ratio of around 0.5 between the annular stress q_{ann} and the CPT cone tip resistance q_c. Yet self-weight penetration is a large displacement event, reaching displacements much higher than typical toe quakes. Therefore, the pile annulus mobilises the full CPT tip resistance in both fine-grained and coarse-grained soils (Chow, 1997; Doherty and Gavin, 2011; Han et al., 2020; Lehane and Gavin, 2001), whereby:

$$q_{ann} = 1.0 q_{c,filter} \quad \text{Equation 2}$$

where $q_{c,filter}$ accounts for geometrical scaling effects between the CPT cone diameter and the annular thickness of the pile using the method by Boulanger and DeJong (2018) and supported by research from Bittar et al. (2022) and Chai et al. (2025). No limiting resistances were applied based on observations from static load tests in Duffy et al. (2024).

2.1.2. Plug resistance in sand and clay

The plug resistance in an open-ended pile comes from friction on the inner pile walls. While this resistance can be significant under static

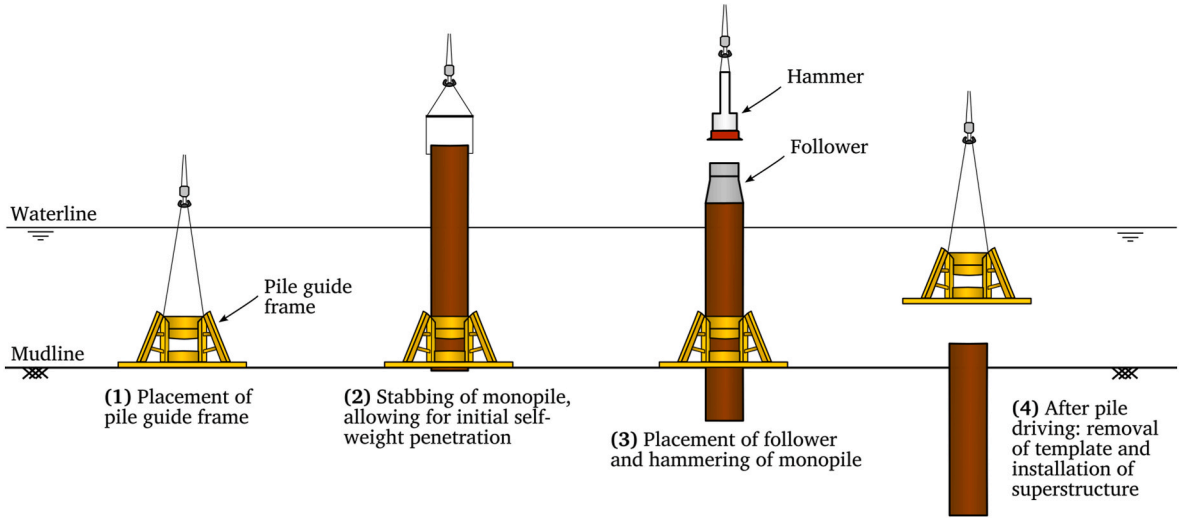

Fig. 1. Example of a monopile installation process.

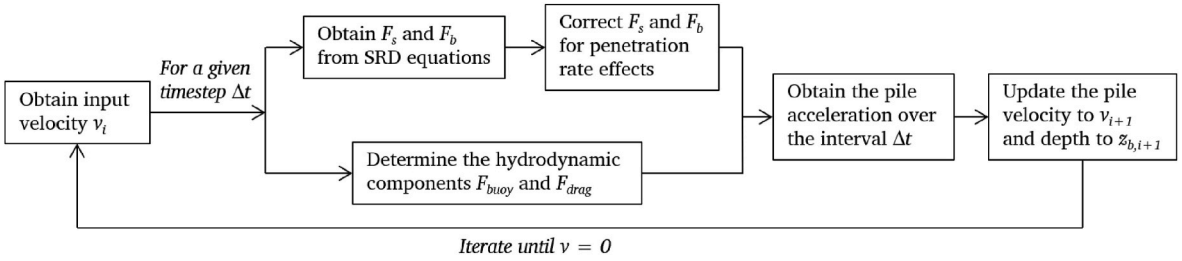

Fig. 2. Summary of the analytical model.

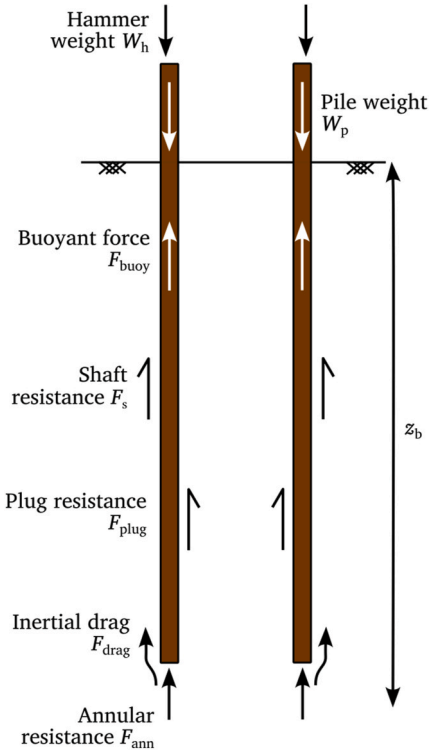

Fig. 3. Forces acting on a pile during self-weight penetration.

loading, a rapidly penetrating pile can cause a phase shift between the accelerations in the pile wall and the accelerations in the soil plug (Liyanapathirana et al., 1998; Randolph, 1987; Smith et al., 1986), whilst also changing the drainage response within the pile plug (Ogawa et al., 2009; Randolph et al., 1991). Consequently, open-ended piles with a diameter greater than 1.5 m are expected to penetrate in a fully coring mode during driving (Lehane et al., 2022a), and by extension, self-weight penetration. For piles with a diameter greater than 750 mm, the contribution of the plug is also expected to be minor.

The plug length ratio *PLR* can be used to describe the plugging behaviour and is expressed as the plug length divided by the embedded pile length. In the Unified clay and sand methods (Lehane et al., 2020, 2022b), the plug length ratio is predicted using:

$$PLR = \tanh\left(0.3^{*}\left(\frac{D_i}{d_{CPT}}\right)^{0.5}\right) \quad \text{Equation 3}$$

where D_i is the inner pile diameter and d_{cpt} is the diameter of the CPT cone—equal to 35 mm for a 10 cm^2 cone.

In sand, Lehane and Gavin (2001) showed that the stress at the base of the soil plug q_p is directly related to the CPT cone resistance and the plug length ratio:

$$q_{plug,sand} = \exp(-2PLR)\,q_c \quad \text{Equation 4}$$

Likewise for clay soils, the Unified clay method takes the results of Doherty and Gavin (2011), who showed that the plug resistance could be modelled using:

$$q_{plug,clay} = \left[0.2 + 0.6\left(1 - PLR\left(\frac{D_i}{D}\right)^2\right)\right] q_t \quad \text{Equation 5}$$

Both Equation (4) and Equation (5) are then used by the analytical model to predict the plug resistance during pile penetration. Just like the annular resistance (Equation (2)), the plug resistance is assumed to be fully mobilised during self-weight penetration and so no reduction factor has been applied to the plug resistances in sand and clay.

2.1.3. Shaft resistance in sand

The Unified pile design method for sand (Lehane et al., 2020) provides an estimate of the pile's shaft capacity using Coulomb's law:

$$q_{s,sand} = (\sigma'_{rc} + \Delta\sigma'_{rd})\tan\delta_f \quad \text{Equation 6}$$

where δ_f is the interface friction angle, taken as 29°, σ'_{rc} is the stationary effective radial stress and $\Delta\sigma'_{rd}$ is the increase in effective radial stress due to dilatancy.

The stationary effective radial stress σ'_{rc} has been correlated to the CPT cone resistance using a database of static load tests (Lehane et al., 2017) performed two weeks after installation on average:

$$\sigma'_{rc} = \left(\frac{q_c}{44}\right)A_{re}^{0.3}\left(\max\left(1, \frac{h}{D}\right)\right)^{-0.4} \quad \text{Equation 7}$$

where A_{re} is the effective area ratio and h is the distance from the pile base. The h/D term accounts for friction fatigue, a phenomenon describing the cyclical reduction in radial stress on the pile caused by pile driving or pile jacking (Gavin and O'Kelly, 2007; Igoe et al., 2011; White and Lehane, 2004). However, the absence of load cycling during self-weight penetration means the magnitude of friction fatigue is not expected to be comparable to a conventional driven pile. Consequently, the analytical model assumes friction fatigue to be negligible during monotonic self-weight penetration and so $\sigma'_{rc} = \left(\frac{q_c}{44}\right)A_{re}^{0.3}$.

Similarly, the increase in radial stress due to dilatancy $\Delta\sigma'_{rd}$ is given by:

$$\Delta\sigma'_{rd} = \left(\frac{q_c}{10}\right)\left(\frac{q_c}{\sigma'_v}\right)^{-0.33}\left(\frac{d_{cpt}}{D}\right) \quad \text{Equation 8}$$

where σ'_v is the vertical effective stress. For most offshore piles, the contribution of $\Delta\sigma'_{rd}$ is small since the pile diameter is many times greater than the CPT diameter.

The Unified method provides the medium-term pile capacity two weeks after installation. However, aging-related increases in shaft resistance are known to occur between installation and static load testing (Gavin et al., 2015; Jardine et al., 2006; Lim and Lehane, 2014;

Rimoy et al., 2015). With this in mind, Lehane et al. (2022a) presented UniSAND-SRD. In short, the UniSAND-SRD method factorises the original shaft resistance formulation by 0.7 to obtain the unaged pile capacity immediately after installation:

$$q_s = 0.7 q_{s,sand} \quad \text{Equation 9}$$

Similar trends were observed in the PAGE dataset where twenty-five open-ended piles were subjected to dynamic load tests immediately after the end-of-driving (Cathie et al., 2023; Scarfone et al., 2023). Furthermore, the same time factor of 0.7 has also shown to be effective in driveability studies by Byrne et al. (2018), Prendergast et al. (2020) and Argyroulis et al. (2024).

2.1.4. Shaft resistance in clay

The Unified method for driven piles in clay (Lehane et al., 2022b) showed that pile capacities were predicted well with the equation:

$$q_{s,clay,uni} = 0.07 F_{st} q_t \max\left[1, \frac{h}{D^*}\right]^{-0.25} \quad \text{Equation 10}$$

where F_{st} is a factor relating to the clay sensitivity and D^* reflects the lower level of displacement induced by an open-ended pile compared to a closed-ended pile and is equal to $(D^2 - D_i^2)^{0.5}$. Similar to the static resistance to driving in sand, the friction fatigue term is not included for self-weight penetration and so $q_{s,clay,uni} = 0.07 F_{st} q_t$.

Yet excess pore pressure development, subsequent equalisation, and post-consolidation aging also affect the shaft resistance in fine-grained soils (Bond and Jardine, 1991; Karlsrud, 2012). Equation (10) estimates a pile's capacity after consolidation, calibrated to a load test database where, on average, 80 % of the excess pore pressures had dissipated around each pile. Yet adjusting Equation (10) to get a static resistance to driving formulation is challenging because of the scarcity of well-instrumented end-of-driving records, particularly in stiff, highly over-consolidated clays (Karlsrud, 2012; Lehane et al., 2022b).

In the context of the Unified method, Jardine (2023) summarises pile tests from Pentre and Tilbrook in low OCR clay and high OCR clay respectively. Measurements one day after installation showed that differences between end-of-driving capacities and the Unified method predictions of 40 % and 70 % for low OCR clay (Pentre) and high OCR clay (Tilbrook) respectively. As a result, these have been used to derive the SRD formulations for the analytical model in clay, resulting in:

$$\text{for NC or low OCR clay} \quad q_{s,clay} = 0.4 q_{s,clay,uni} \quad \text{Equation 11}$$

$$\text{for high OCR clay} \quad q_{s,clay} = 0.7 q_{s,clay,uni} \quad \text{Equation 12}$$

2.2. Penetration rate effects

The SRD formulations give the static pile capacity instantaneously at the end-of-driving. However, the dynamic nature of self-weight penetration requires a correction for the differences between a pile's velocity during a load test (penetrating at several centimetres per day) and one experiencing pile run (more than 1 m/s). Finnie and Randolph (1994) proposed that the resistance acting on a penetrometer depends on the normalised velocity V, expressed as:

$$V = \frac{vD}{c_h} \quad \text{Equation 13}$$

where c_h is the coefficient of consolidation in the horizontal direction. The transition from drained to partially drained conditions occurs at normalised velocities of around 0.1, and then goes from partially drained to undrained when V exceeds 30 (Colreavy et al., 2016).

Penetrating at a velocity of 0.02 m/s, the behaviour of a CPT in clay is undrained—just like the self-weight penetration of a pile—so no correction was applied to the SRD formulations in clay. In sand, however, the normalised velocity of a fully coring pile induces undrained or partially drained penetration (Holeyman, 1992; Hölscher et al., 2012; Huy, 2008), unlike the response of a CPT in sand which behaves as fully drained. Therefore, the analytical model applies a correction to the CPT-based SRD method to account for the differences in drainage conditions between CPT and pile penetration in sand.

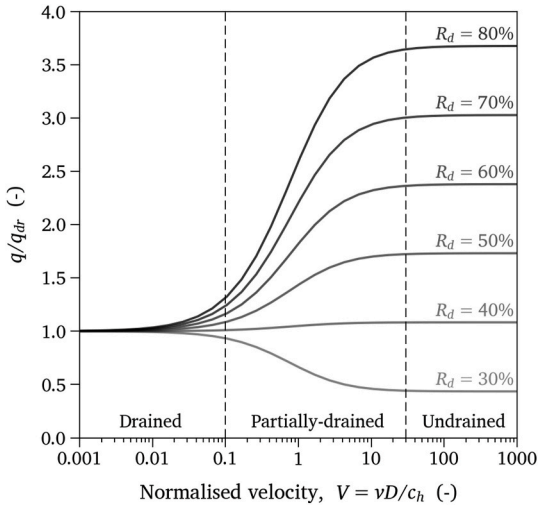

Fig. 4. Change in normalised penetrometer resistance from drained to undrained conditions.

Comparing penetrometers at slow speeds (drained conditions) and high speeds (undrained conditions) in sand, several researchers (Chow et al., 2018; Danziger and Lunne, 2012; Hölscher et al., 2012; Huy, 2008; Silva, 2005; Suzuki, 2015; White et al., 2018) have shown that the resistance on a penetrometer is a function of the sand's contractile/dilatant behaviour, which itself varies with sand density, mineralogy and stress level (Bolton, 1986). In loose sand, rapid penetration briefly increases porewater pressures surrounding the penetrometer, reducing the in-situ effective stresses and the resistance acting on the penetrometer. Conversely, dense to very dense sands exhibit a dilatant response upon shearing, creating negative pore water pressures, higher effective stresses and increasing the resistance acting on the penetrometer.

To quantify the change in resistance under rapid penetration, several authors (Ayala et al., 2023; Chow et al., 2018, 2020; Lehane, 2024; Randolph and Hope, 2004; Robinson and Brown, 2013; Suzuki, 2015; White et al., 2018) proposed an equation of the form:

$$\frac{q}{q_{dr}} = \frac{q_{un}}{q_{dr}} + \frac{1 - q_{un}/q_{dr}}{1 + (V/V_{50})^c} \quad \text{Equation 14}$$

where q_{dr} is the drained resistance, q_{un} is the undrained resistance, c is a fitting parameter describing the degradation in q_c from undrained to drained conditions (taken as 1.3 for a penetrometer as per Chow et al. (2018)), and V_{50} is the normalised velocity at 50 % consolidation and is roughly equal to 1 (Randolph and Hope, 2004).

For high-speed pile penetration, the ratio of undrained to drained resistance q_{un}/q_{dr} is the governing parameter in Equation (14). In sand, q_{dr} is obtained directly from standard CPT penetration. However, q_{un} is much more challenging to determine because of the difficulty in reaching sufficiently high penetration velocities and measurement frequencies in instrumented models (Chow et al., 2018; Lehane, 2024; Suzuki, 2015). Difficulties in obtaining representative, undisturbed sand samples means there's also a lack of understanding for sand-specific cone factors (N_{kt}) that correlate q_c to the undrained shear strength s_u (Kaltekis and Peuchen, 2022; White et al., 2018).

One of the few efforts to quantify q_{un}/q_{dr} come from Chow et al. (2018), who found q_{un}/q_{dr} values of 0.5 and 4 in loose (D_R = 31 %) and

dense sand ($D_R = 85$ %) respectively. For the purposes of the analytical model, these have been taken as limiting values with linear interpolation for intermediate relative densities (Fig. 4). The ratio between the drained (static) resistance and the undrained resistance was then applied to both the base and the shaft resistances to get the dynamic resistance to driving.

There are two limitations to Fig. 4 which have not been considered in the model: cavitation and viscous effects. In dilatant soils at shallow water depths, cavitation will limit how much negative excess pore water pressures can develop, thus also limiting the rate-induced increase in radial stress. However, precisely quantifying the effect of cavitation is challenging (Cathie et al., 2020; Chow et al., 2022; Randolph et al., 2018; Roy et al., 2022) because of the complex pore pressure field around the pile, where the surrounding soil exhibits different stages of compression, extension and shearing (Hölscher et al., 2012; White, 2002).

Viscous effects can be modelled by including an additional term to Equation (14) (e.g. Chow et al. (2018); Lehane et al. (2009); Zhu and Randolph (2011)). In sand, viscous effects are expected to be relatively minor compared to consolidation effects (Chow et al., 2020) and in clays, viscous effects begin to take effect at high normalised velocities (Lehane et al., 2009; Suzuki, 2015). However, its contribution in the context of uncontrolled pile penetration is expected to be low and has therefore not been considered in the analytical model.

For intermediate soils like silts or interlaminated deposits, changes in penetration resistance are difficult to define since the drainage conditions around the CPT and the pile are often unknown, exacerbated by the fact that the normalised velocity can fall in the partially drained zone ($0.1 \leq V \leq 30$). Intermediate soils should therefore be examined on a case-by-case basis, with particular attention to the soil's coefficient of consolidation and the probe diameter (Equation (13)) to check if undrained, partially-drained or fully drained penetration is occurring. Dissipation tests and variable rate CPTs (DeJong and Randolph, 2012; Jaeger et al., 2010; Lehane, 2024) can be especially useful in this context, particularly with clarifying the drainage response and how the soil's resistance changes with increasing penetration velocity (i.e. c and V_{50} from Equation (14)).

2.3. Hydrodynamic components

Buoyant forces act in opposition to the downward momentum of the penetrating pile. As more and more of the pile submerges, a buoyant force acts on the pile that corresponds to the volume of water displaced by the pile, in other words, the pile's effective weight W'_p. Likewise, soil is also displaced during this process, corresponding to the effective unit weight of the displaced soil. Both buoyancy components have been combined into a single term F_{buoy}. Buoyant effects are particularly relevant for integrated structures where the foundations are integrated directly into the superstructure, like in skirted jackets or monopile towers.

Inertial drag also acts in opposition to the penetrating pile, described in a series of small-scale tests on dynamically installed anchors (O'Loughlin et al., 2013). Nevertheless, inertial drag is generally considered to be negligible in sand (Dayal and Allen, 1975) and has not been presented further in this paper after initial model simulations showed it to also be negligible for the database cases.

2.4. Initial velocity

For each self-weight penetration case in this paper, the initial velocity is set to zero. However, instances of pile run during pile driving can also be assessed by assuming the imparted energy from the hammer is transformed into the kinetic energy of pile-hammer system (Sun et al., 2022):

$$v = \sqrt{\frac{2\eta f E}{m_p + m_h}} \qquad \text{Equation 15}$$

where η is the efficiency of the pile-hammer system, f is the hammer efficiency and E is the imparted energy from the hammer. For more complex analyses, 1D wave equation-based models are recommended to better capture the energy transfer mechanisms from hammer-to-pile and from pile-to-soil.

3. Self-weight penetration database

The majority of the self-weight penetration database (Table 1) was compiled by Shell UK, part of which was previously used by Overy (2007), Byrne et al. (2018) and Prendergast et al. (2020) to analyse pile driveability methods. These records consist of monopile and jacket pile installations from across the North Sea. At each site, the pile were installed following the procedure in Fig. 1 where the piles were allowed to penetrate entirely under their own self-weight, resulting in the self-weight penetrations shown in Table 1. A follower and a hammer were then placed on the pile, often starting even more self-weight penetration, and then pile driving was performed. Additional records from public sources have also been included in the database: South China Sea (Sun et al., 2022) and the Taiwan Strait (Thijssen and Roelen, 2024).

The pile diameters range from 2.1 to 4.2 m, with pile weights ranging from 1.6 to 6.3 MN (160–632 tonnes). At least one CPT and borehole was available at each location and CPT-based correlations were used to cross-check the derived soil parameters and to deduce the relative density and the soil's dilatant/contractile response as per Robertson (2021). Where available, laboratory tests (oedometer, triaxial, particle size distribution tests) were used to obtain the coefficient of consolidation, over-consolidation ratio and cross-check the CPT-based correlations.

Most of the database records are typical silica sand and clay soils. Caravel, Goldeneye and Shamrock can be considered as conventional self-weight penetration scenarios (Fig. 5), where the pile easily penetrated through soft or loose seabed sediment, coming to rest in an underlying dense sand layer. At Cutter, K17 and L09, dense sand is present at very shallow depths, and correspondingly, self-weight penetration was only a couple of metres into the sand the sand layer. At Shearwater, self-weight penetration occurs in stiff, over-consolidated clay where q_c measured 1 MPa across the penetration depth.

Intermediate or mixed soils, like clayey sand, sandy clay or silt are seldom present across the database cases, with only the surficial layer of sandy silt at the Taiwan Strait and the highly interlayered soils in the South China Sea. Both plasticity tests and the soil behaviour type index (Robertson, 2010) suggested that no sensitive or organic soils were present across any of the cases.

Table 1
Database of offshore self-weight penetration records.

Site	Pile	Ground conditions over SWP depth	Water depth (m)	Total pile length (m)	Diameter (m)	Weight (MN)	Self-weight penetration (m)
Caravel	P1	Loose sand over soft clay and very dense sand	31	40	4.2	2.4	8.2
Cutter	P1	Medium dense sand	32	43	4.2	2.2	2.8
Goldeneye	B1-1	Very soft clay over dense sand	120	62	2.1	1.6	10.0
K17	P1	Dense sand with stiff clay bed	29	42	4.2	2.2	2.7
L09	FA1	Dense sand	24	43	4.2	2.7	2.0
L09	FB1	Dense sand	21	40	4.2	2.2	2.5
Shamrock	P1	Loose sand over soft clay and dense sand	30	43	4.2	2.7	8.8
Shearwater	P1	Firm to stiff clay over very stiff clay	90	72	2.1	2.5	8.0
South China Sea	P1	Interlayered loose sand and silty clay	191	158	2.7	6.3	12.0
Taiwan Strait	P1-1	Sandy silt over loose sand	35	95	3.5	2.8	9.0
Taiwan Strait	P3-3	Sandy silt over loose sand	35	95	3.5	2.8	7.0

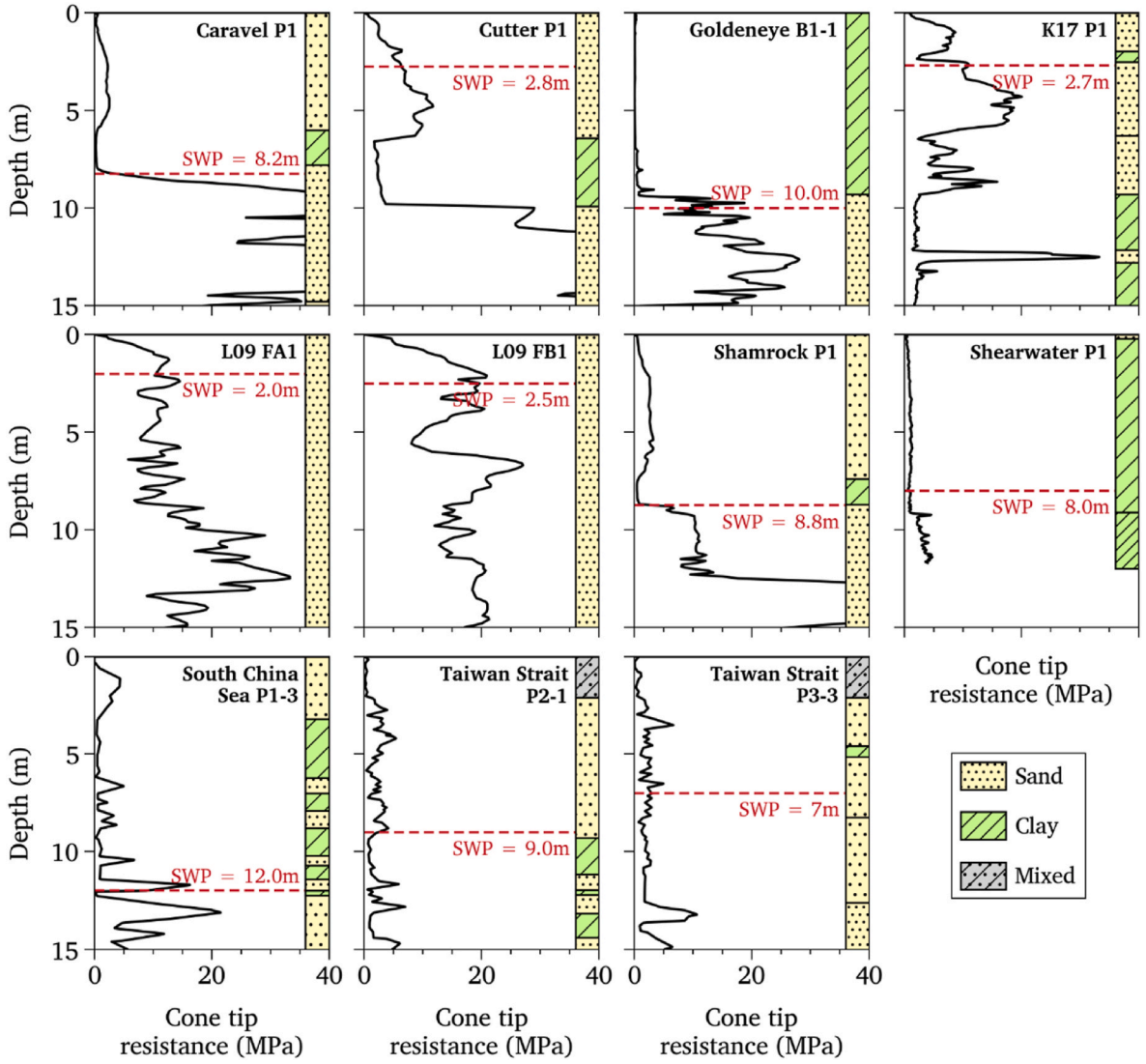

Fig. 5. CPTs from each location with the measured self-weight penetration (SWP).

4. Results

Table 2 and Fig. 6 summarise the predicted self-weight penetrations, along with the site-by-site results in Appendix A. For reference, a "static prediction" has been included, defined as the first depth at which the unfactored SRD (F_b and F_s) exceeds the combined effective weight of the pile and hammer assembly.

The model's predictive accuracy, quantified using the root mean squared error (RMSE), is 1.5 m across the dataset. Most of the error comes from sites where penetration into the near-surface medium dense to dense sand layers is shallow—particularly at Cutter, K17 and L09. At these sites, the model systematically underestimates the amount of self-weight penetration, predicting little to no penetration into the sand. This underestimation may be caused by the base resistance formulation

Table 2
Predictions of self-weight penetration depth by the analytical model.

Site	Pile	Measured SWP (m)	Static prediction (m)	Analytical model prediction (m)	Error (m)	Error (%)
Caravel	P1	8.2	1.3	8.3	+0.1	+1 %
Cutter	P1	2.8	0.5	0.5	−2.3	−82 %
Goldeneye	B1-1	10.0	8.1	9.7	−0.3	−3 %
K17	P1	2.7	0.0	0.0	−2.7	−100 %
L09	FA1	2.0	0.5	0.5	−1.5	−75 %
L09	FB1	2.5	0.5	0.5	−2.0	−80 %
Shamrock	P1	8.8	1.1	9.2	+0.4	+5 %
Shearwater	P1	8.0	4.2	8.2	+0.2	+2 %
South China Sea	P1-3	12.0	1.0	13.1	+1.1	+9 %
Taiwan Strait	P2-1	9.0	2.2	11.1	+2.1	+23 %
Taiwan Strait	P3-3	7.0	2.2	7.1	+0.1	+1 %
				Mean	**−0.4**	**−27 %**
				Std. Dev.	**1.5**	**46 %**

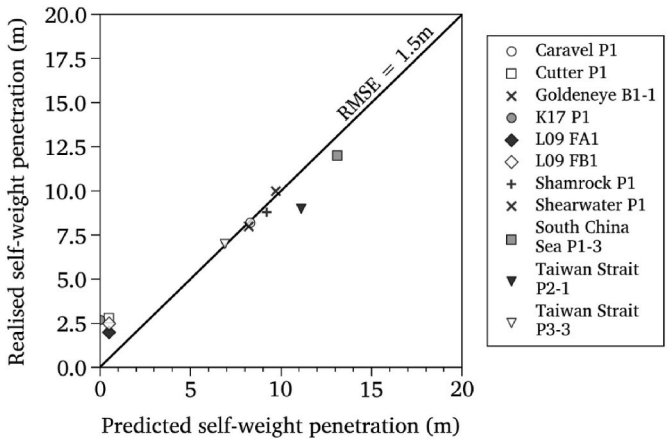

Fig. 6. Predictions of the analytical model compared to measured self-weight penetrations.

(Equation (2)), which does not explicitly account for shallow failure mechanisms at these depths. These mechanisms can lead to lower-than-expected base capacities, ultimately affecting the model's ability to predict self-weight penetration at shallow depths. Additional influences may include shallow penetration effects on the CPT (Puech and Foray, 2002) and construction-related variations such as partial initial embedment, inclination in the pile or topographical irregularities.

For the seven piles which penetrated beyond 5 m, the model shows good accuracy across the different soil conditions: with an average error equal to 0.5 m (5 %) and a standard deviation of 0.8 m (9 %). In loose overlying sand, like at Caravel or Shamrock, the rate effect correction (Equation (14)) usually resulted in a reduction in the resistance acting on the pile. Correspondingly the static prediction consistently underestimated the self-weight penetration at these sites because of the lack of a rate-dependent term. As the pile approached deep, dense to very dense sand layers—like at Caravel, Goldeneye or Shamrock—further self-weight penetration is limited. This occurs regardless of whether a rate effect reduction factor is used because the base resistance provided from the dilative, denser layers already tend to dominate, therefore limiting any further penetration.

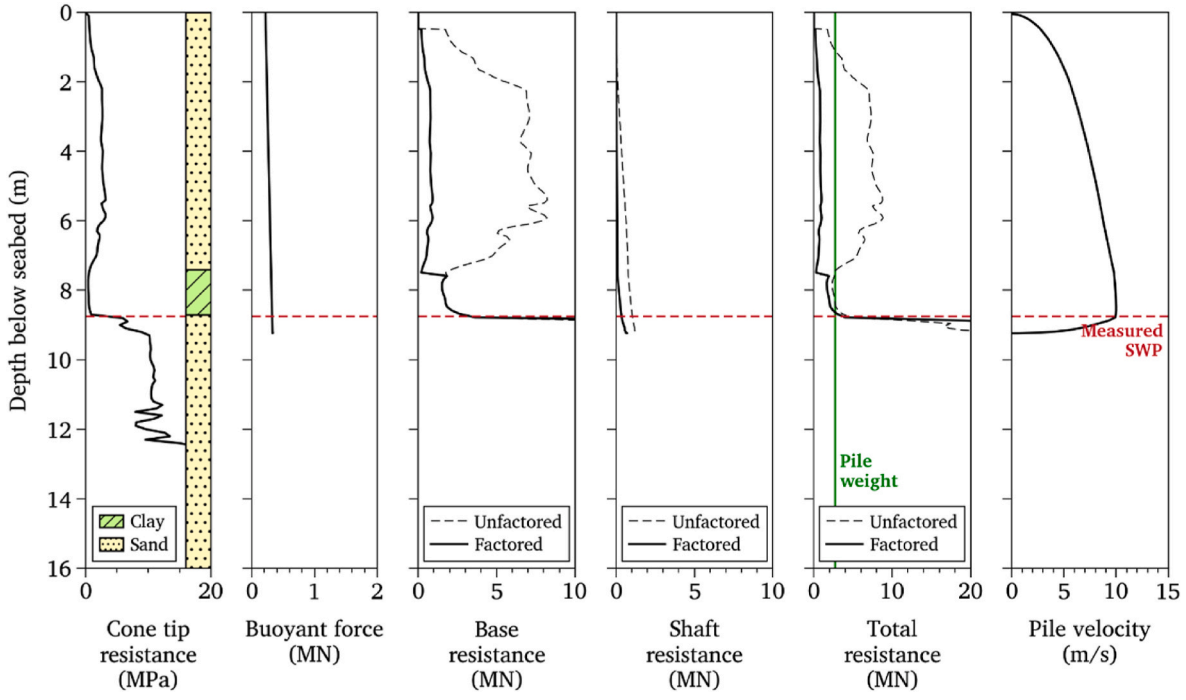

Fig. 7. Example of the analytical model predictions for Shamrock P1.

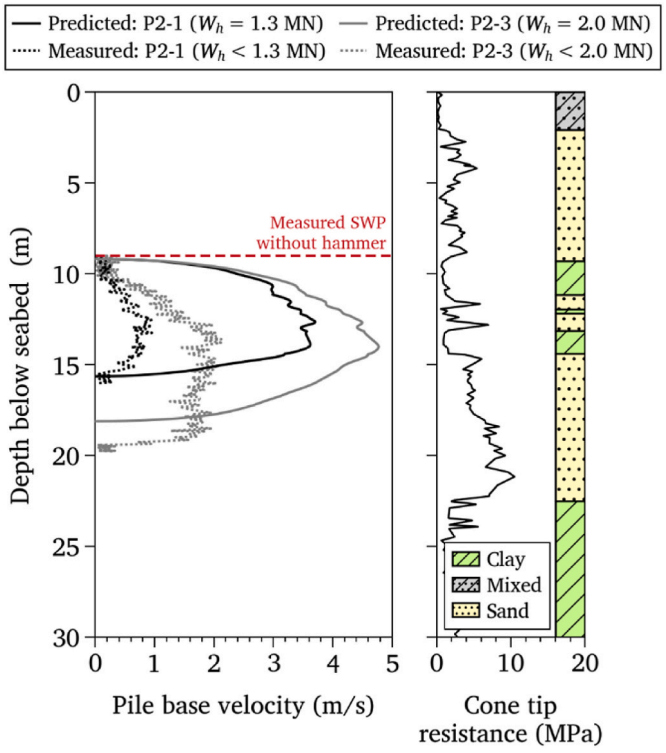

Fig. 8. Influence of hammer placement on piles P2-1 and P2-3 from Thijssen and Roelen (2024).

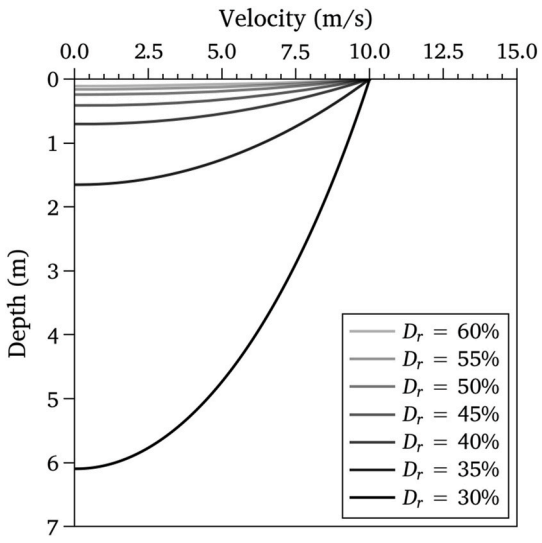

Fig. 9. Penetration of a monopile (D = 4.2 m; W_p= 2.4 MN) into a synthetic, homogeneous sand layer of varying relative densities. No shaft resistances above the layer have been considered.

4.1. Example from a single site

To give an illustrative example (Fig. 7), pile P1 at Shamrock was a 4.2 m diameter monopile weighing 2.4 MN, installed in 2007 as part of the construction of a gas platform in the North Sea. The uppermost layer at Shamrock consists of 7 m of loose sand and lies above a 2-m-thick bed of soft clay with average q_c values of 0.6 MPa. Below this clay bed is a medium dense sand layer with average q_c values of 10 MPa. Self-weight penetration of the monopile stopped near the top of the medium dense sand layer.

The analytical model overpredicts the self-weight penetration of P1 by 0.4 m (≈5 %) (Fig. 7). The model predicted a peak velocity of 11 m/s just above the medium dense sand layer, with the pile's momentum allowing penetration to continue 1 m into the medium dense sand. The pile's acceleration means penetration is mostly undrained across the self-weight penetration depth (in terms of the normalised velocity, Fig. 4). As a result, both the base and shaft resistances in the overlying loose sand were factored down from the original SRD resistance (Equation (9) and Equation (11) respectively). The buoyant force at Shamrock, like most of database cases, has a minor influence on the self-weight penetration, amounting to a maximum upward force of 0.4 MN.

4.2. Comparison with velocity measurements

Thijssen and Roelen (2024) present one of the few published cases of an uncontrolled penetration event with velocity measurements. The study looks at 3.5 m diameter piles installed at several jacket locations in the Taiwan Strait, with each pile weighing 2.7 MN.

At jacket location #2, all three piles (referred to as piles P2-1, P2-2, P2-3 in this paper) penetrated 8–9 m under self-weight alone, 2.1 m less than predicted by the analytical model (Table 2). Afterwards, a hammer weighing 2.9 MN was slowly placed onto the pile head, initiating further self-weight penetration. Two piles (P2-1 and P2-2) penetrated a further 12 m while pile P2-3 penetrated an additional 7 m. Penetration velocities were derived from video footage of the installations. Crane load measurements showed that pile run began once the hammer weight W_h reached 1.3 MN and 2.0 MN (48 % and 74 % of the total hammer weight) for piles P2-1 and P3-3 respectively. Penetration velocities reached 1–2 m/s for both piles, from which the normalised velocities indicated strongly undrained behaviour ($V \gg 100$). During both episodes of pile run, the weight of the hammer transferred back to the crane rigging, progressively reducing the hammer's weight on top of the pile.

For simplicity, the analytical model considered the inputted hammer weight W_h as a constant across the full self-weight penetration depth, set at the maximum hammer weight prior to pile run. The onset of pile run was well anticipated by the analytical model (Fig. 8) and the extent of the penetration event was also relatively well predicted. However, the velocities tend to be overpredicted compared to the measured velocities, partly because of the simplifying assumption of taking the hammer weight as a constant. Contrary to the overpredictions of the initial self-weight penetration in the surficial loose sand layer, the underprediction of the pile run's extent through the medium dense sand layer suggests that further work is needed in understanding the ratio of undrained to drained resistance in Fig. 4 and its effect on the pile's annular resistance.

4.3. Influence of penetration rate correction

To elaborate on how volumetric changes affect the penetration resistance, Fig. 9 shows the model's prediction for a monopile (with the same dimensions as Caravel P1) penetrating into a homogeneous sand sample at an entry velocity of 10 m/s. Unsurprisingly, the deepest penetration occurs in loose sand with a relative density D_r of 30 %. At this relative density, the rate effect model (Fig. 4) assumes that the sand contracts upon shearing, initiating a build-up of porewater pressure and reducing the resistance on the pile by 50 %.

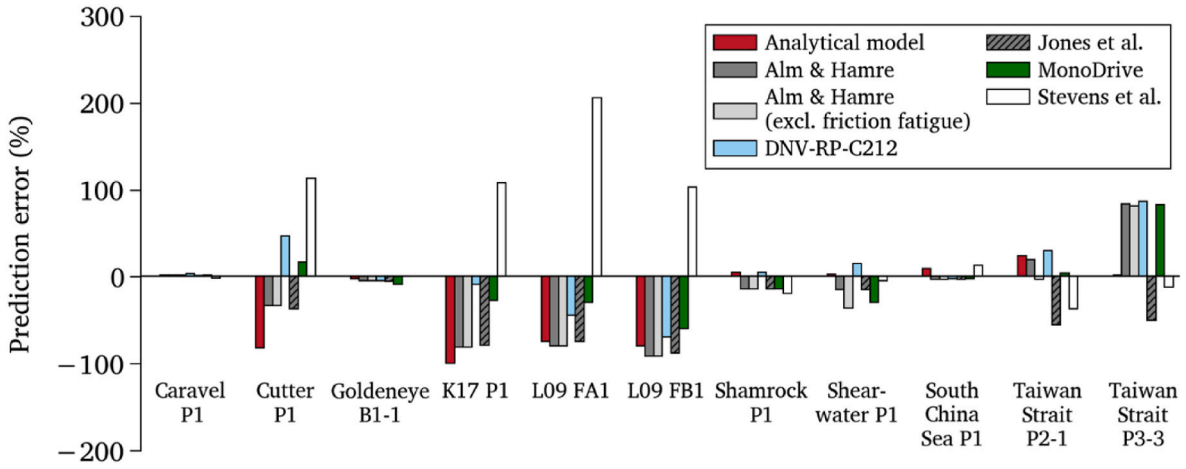

Fig. 10. Predictions of the analytical model compared to other SRD methods.

Table 3
Statistical summary of the self-weight penetration results.

	Mean error (m)	Std. dev. (m)	MAE (m)	RMSE (m)
Analytical model	−0.44	1.50	1.16	1.50
Alm & Hamre	−0.26	2.32	1.66	2.23
Alm & Hamre (excl. friction fatigue)	−0.61	2.29	1.66	2.27
DNV-RP-C212	+0.74	2.13	1.42	2.16
Jones et al.	−1.72	1.47	1.73	2.22
MonoDrive	−0.11	2.12	1.32	2.02
Stevens et al.	+0.70	2.33	1.90	2.33

The transition point from contractile to dilatant behaviour occurs at a relative density of 40 %. With the resistance now increasing relative to the static drained resistance, the pile quickly decelerates within the first 2 m, primarily because of the base contribution of the pile annulus. The example shows the sensitivity of the model to the density variations—and by extension its volumetric behaviour—on the predictions of the analytical model, similar to what's been shown for free-fall penetrometers (White et al., 2018). Identifying the transition from contractile to dilatant behaviour is therefore a critical element in estimating the likelihood of pile run, particularly in terms of the relative change in pile resistance during undrained penetration.

4.4. Comparison with industry practice

In practice, the predicted self-weight penetration is often designated as the depth at which the effective weight of the pile/hammer system is equal to the upward resistance, determined using a static resistance to driving method (Shonberg et al., 2017). To compare the analytical model to existing practice, five different SRD methods have been used.

- Alm and Hamre (2001): CPT-based method developed from installations across the North Sea, with diameters ranging from 1.8 m to 2.8 m. The method also incorporates a depth-dependent term to account for friction fatigue, similar to Equation (8). Given that piles undergoing self-weight penetration have not been subjected to the same cyclical loading as driven piles, this comparison has considered the SRD method both with and without the friction fatigue term.
- **DNV-RP-C212** (DNV, 2019): CPT-based approach based on a back-analysis by Lunne and Kvalstad (1982) of thirteen skirted foundation installations in dense sands and over-consolidated stiff clays in the North Sea. For this analysis, the most probable estimate was taken.
- Jones et al. (2020): Modification of the Alm and Hamre (2001) method using an installation database of 277 piles from 34 sites across the world, with diameters ranging from 0.66 m to 6.5 m. The modification is cited to improve predictions in heavily over-consolidated clay, with comparable performance in other soil conditions.
- **MonoDrive** (Perikleous et al., 2023; Stergiou et al., 2023): CPT-based approach developed from installation records across thirteen sites in the North Sea and Irish Sea, with diameters ranging from 5.60 m to 8.40 m. Six fitting parameters are included in the model, each calibrated against the database whilst also providing scope for site-specific calibration.

Table 4
Predicted self-weight penetration depths by different SRD methods. All units are in metres below seabed level.

Site	Pile	Measured	Alm and Hamre		DNV-RP-C212	Jones et al.	Mono-Drive	Stevens et al.
			Including friction fatigue	Excluding friction fatigue				
Caravel	P1	8.2	8.3	8.3	8.5	8.3	8.3	8.1
Cutter	P1	2.8	1.9	1.9	4.1	1.8	3.3	6.0
Goldeneye	B1-1	10.0	9.5	9.5	9.5	9.5	9.1	10.0
K17	P1	2.7	0.5	0.5	2.5	0.6	2.0	5.6
L09	FA1	2.0	0.4	0.4	1.1	0.5	1.4	6.1
L09	FB1	2.5	0.2	0.2	0.8	0.3	1.0	5.1
Shamrock	P1	8.8	7.5	7.5	9.2	7.5	7.5	7.1
Shearwater	P1	8.0	6.8	5.1	9.2	6.8	5.6	7.6
South China Sea	P1-3	12.0	11.6	11.6	11.7	11.6	11.7	13.6
Taiwan Strait	P2-1	9.0	10.8	8.7	11.7	4.0	9.4	5.6
Taiwan Strait	P3-3	7.0	12.9	12.7	13.1	3.5	13.0	6.2

- Stevens et al. (1982): Developed from an installation database of 1-m-diameter piles in the Arabian Gulf. The method is similar to the effective stress method for sand in API (2011) along with the total stress method proposed for clays by Semple and Gemeinhardt (1981). Given the size of the piles in the self-weight penetration database, a fully-coring pile is assumed and therefore the upper bound method in Stevens et al. (1982) has been taken, which assumes equal shaft resistances both inside and outside the pile wall.

A summary of the predictions are shown in Fig. 10 and Table 3, along with the complete results in Table 4. These results are quantified in terms of the error (where a positive error represents an overprediction and a prediction deeper than the measured penetration), the mean absolute error (MAE) and the root mean squared error (RMSE). Generally, the extent of self-weight penetration tended to be underestimated by most SRD methods, except for DNV-RP-C212 and Stevens et al. (1982). Of all the methods, the analytical model had the lowest MAE and RMSE, outperforming the next best performing method by 28 % in terms of the RMSE. Conversely, the method by Stevens et al. (1982) had the highest MAE and RMSE.

Most of the error in the prediction methods was concentrated at sites K17 and L09, where the surficial dense sand layer led to six of the seven methods predicting a self-weight penetration shallower than what was measured. The method by Stevens et al. (1982) overestimated the self-weight penetration at these two sites, largely because of the dependency of the method on the in-situ effective stress σ'_v—thus resulting in substantial deviations from the other methods at shallow depths.

Four of the five SRD methods were calibrated on pile driving records as opposed to monotonic self-weight penetration events. Three of these methods (Alm and Hamre, Jones et al. and MonoDrive) include a friction fatigue term to account for the degradation of shaft resistance under cyclical hammer loading, similar to Equation (7). Taking the Alm and Hamre (2001) method as an example, removing the friction fatigue term only had a minor effect on the predictions, with the influence of the term only taking effect at deeper self-weight penetration depths and where the shaft resistance contributed substantially to the total resistance, such as at Shearwater or the Taiwan Strait. These same results were also shown by excluding the friction fatigue term in the Jones et al. (2020) and MonoDrive methods (not included for brevity).

5. Conclusion

This paper has provided a framework for modelling a pile's dynamic resistance during self-weight penetration and pile run, as well as the energy stored in the pile-hammer system. The model incorporates novel CPT-based static resistance to driving formulations into a conservation of energy equation, allowing for the pile's resistance to be updated based on the velocity of the pile. The model predictions were benchmarked against a database of self-weight penetration records across a range of soil conditions, including soft to stiff clay and loose to very dense sand. Compared to five industry-standard methods, the proposed model showed improved performance, reducing the root-mean-square error by 26 % compared to the next best approach.

However, the model's sensitivity to the inputted relative density highlights the importance of accurately characterising the sand's in-situ volumetric response. Future research should expand the dataset with velocity measurements of self-weight penetration to better understand how the penetration velocity affects a pile's base and shaft resistance. Moreover, the paper has only considered the analytical model for self-weight penetration events. To forecast pile run events during installation, incorporating either a simple energy-transfer equation (e.g. Equation (15)) or more complex driveability models would be needed. With this, the analytical model brings possibilities for digital twinning the entire installation process itself, for example, by integrating crane load data, driving records, and pore pressure dissipation to better model installation delays and to understand energy transfer from the pile to the crane rigging.

CRediT authorship contribution statement

Kevin Duffy: Writing – review & editing, Writing – original draft, Software, Investigation, Formal analysis, Data curation, Conceptualization. **Cormac Reale:** Writing – review & editing, Software, Methodology. **Ken Gavin:** Writing – review & editing, Supervision, Conceptualization.

Data availability statement

The data that supports the findings of this study are available from the corresponding author upon reasonable request.

Declaration of competing interest

The authors declare that they have no known competing financial interests or personal relationships that could have appeared to influence the work reported in this paper.

Acknowledgements

The first author was supported by the Dutch Research Council (NWO) on the Urbiquay STABILITY project (NWA.1431.20.004).

APPENDIX A. Results for each site

This appendix presents the output of the analytical model for each site, showing the contribution of the static resistance to driving (both unfactored and factored, as per Fig. 4), along with the upward buoyant contribution.

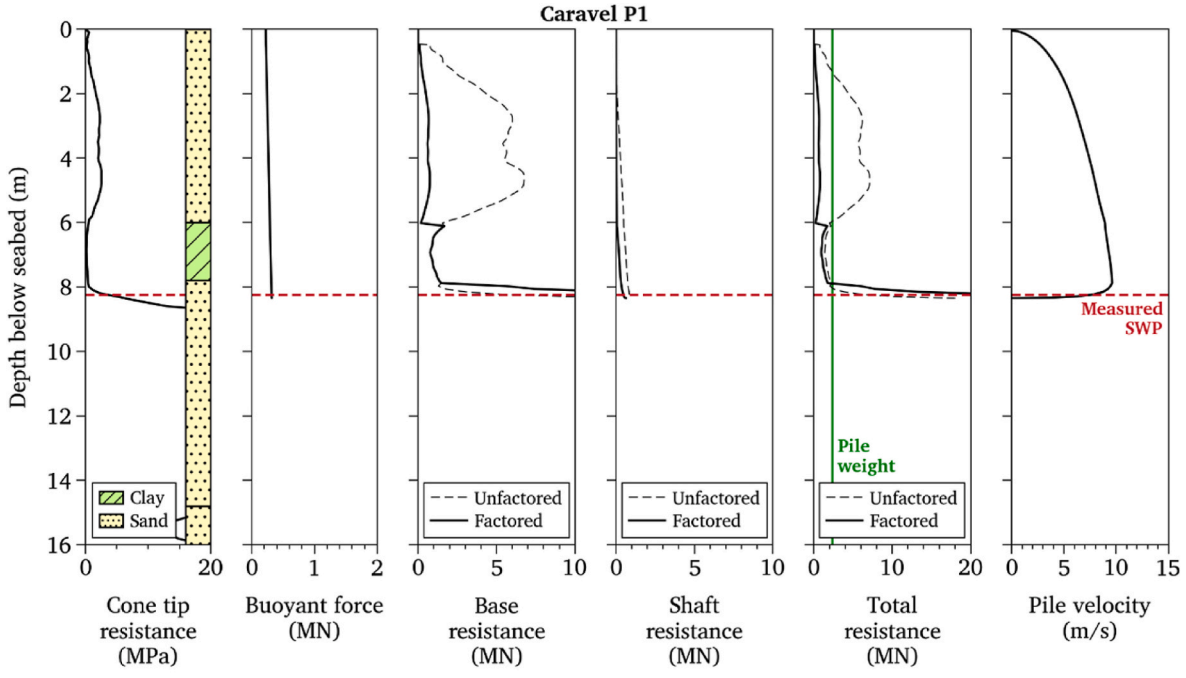
Caravel P1
Depth below seabed (m)
Clay
Sand
Cone tip resistance (MPa)
Buoyant force (MN)
Base resistance (MN)
Shaft resistance (MN)
Total resistance (MN)
Pile velocity (m/s)
Unfactored
Factored
Pile weight
Measured SWP

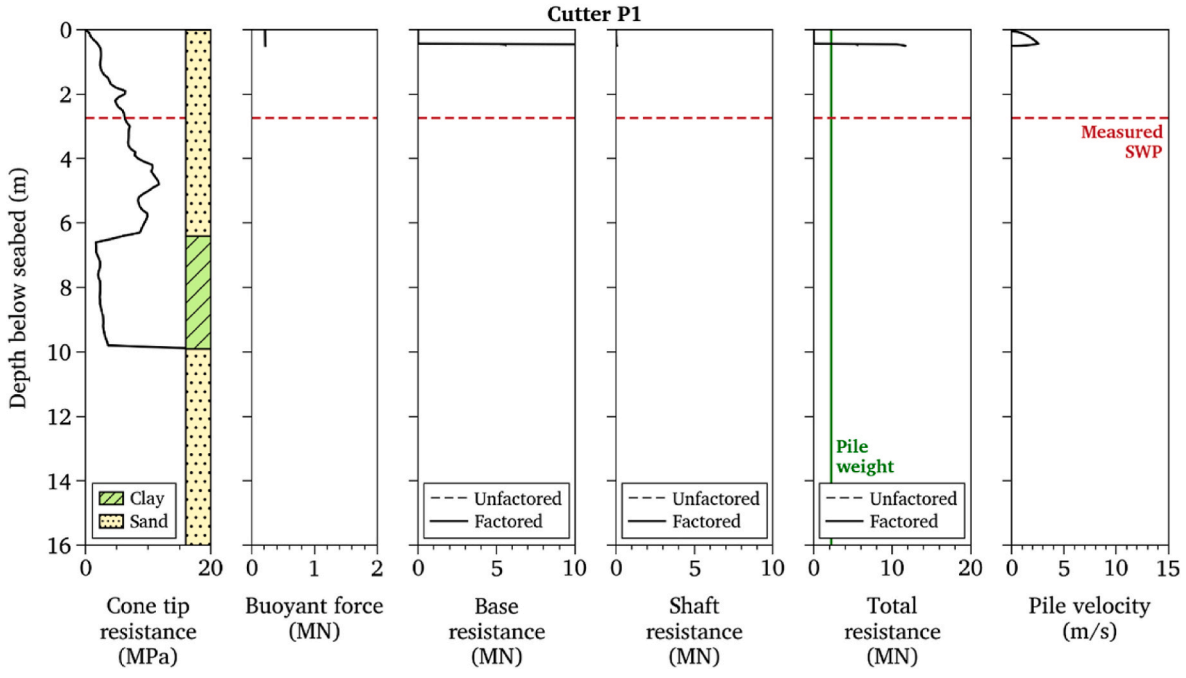
Cutter P1
Depth below seabed (m)
Clay
Sand
Cone tip resistance (MPa)
Buoyant force (MN)
Base resistance (MN)
Shaft resistance (MN)
Total resistance (MN)
Pile velocity (m/s)
Unfactored
Factored
Pile weight
Measured SWP

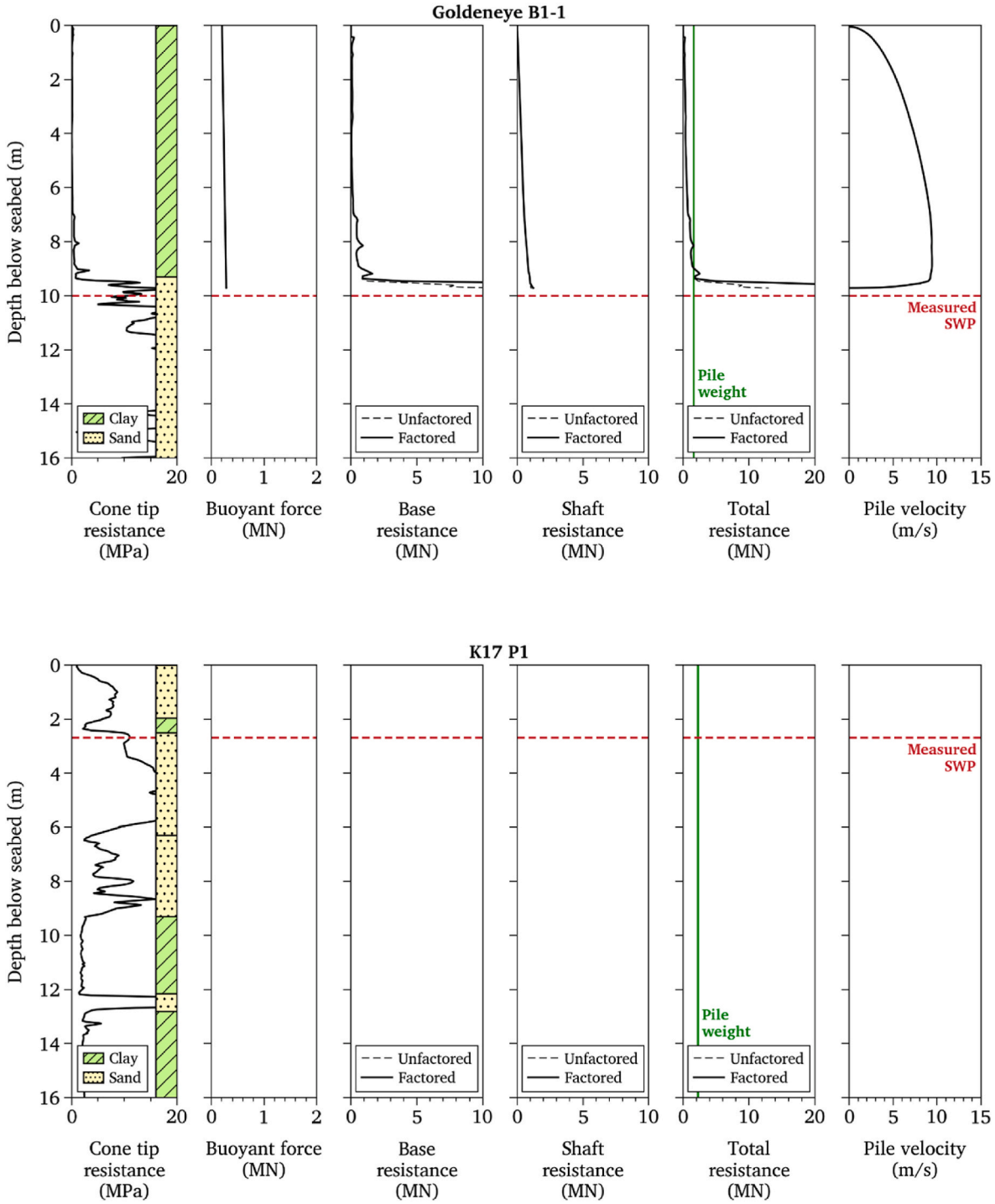
Goldeneye B1-1
Depth below seabed (m)
Clay
Sand
Cone tip resistance (MPa)
Buoyant force (MN)
Unfactored
Factored
Base resistance (MN)
Shaft resistance (MN)
Pile weight
Total resistance (MN)
Measured SWP
Pile velocity (m/s)
K17 P1
Depth below seabed (m)
Clay
Sand
Cone tip resistance (MPa)
Buoyant force (MN)
Unfactored
Factored
Base resistance (MN)
Shaft resistance (MN)
Pile weight
Total resistance (MN)
Measured SWP
Pile velocity (m/s)

. (*continued*).

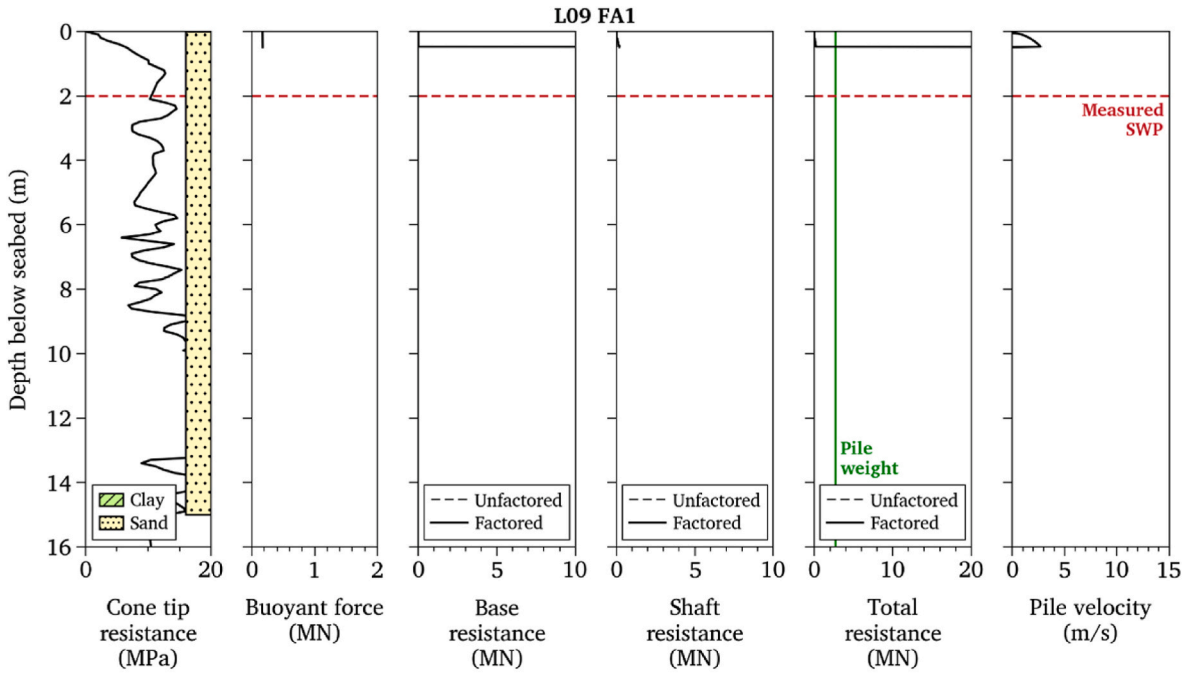
L09 FA1
Depth below seabed (m)
Clay
Sand
Cone tip resistance (MPa)
Buoyant force (MN)
Unfactored
Factored
Base resistance (MN)
Shaft resistance (MN)
Pile weight
Total resistance (MN)
Measured SWP
Pile velocity (m/s)

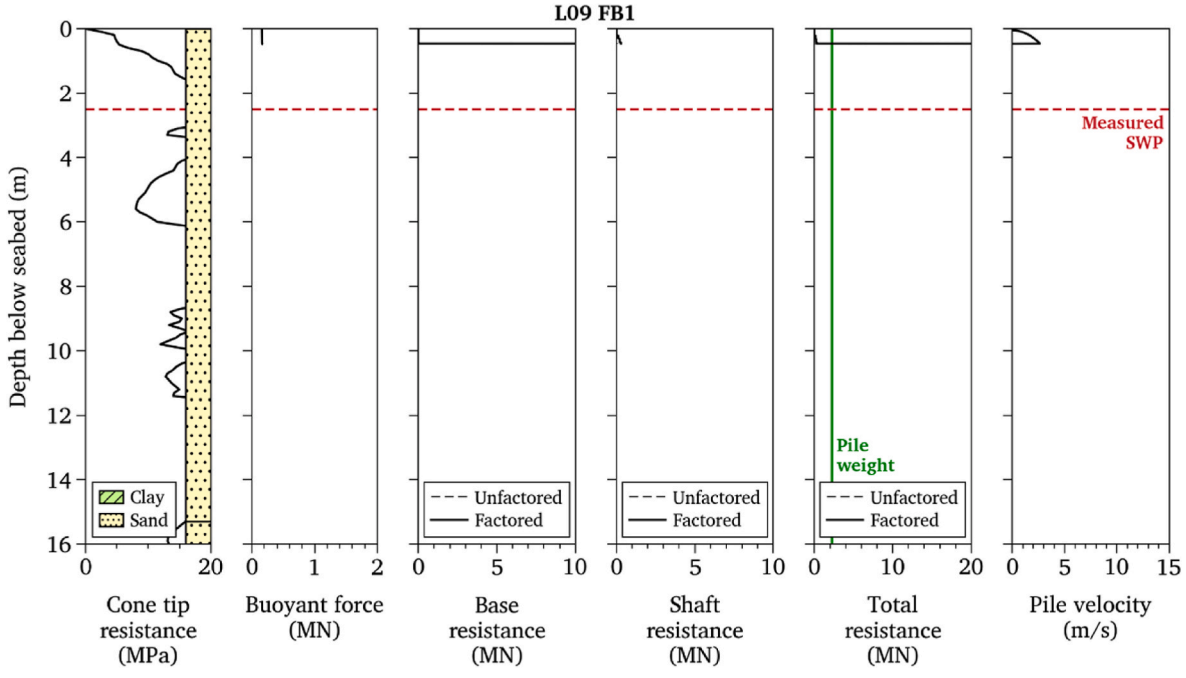
L09 FB1
Depth below seabed (m)
Clay
Sand
Cone tip resistance (MPa)
Buoyant force (MN)
Unfactored
Factored
Base resistance (MN)
Shaft resistance (MN)
Pile weight
Total resistance (MN)
Measured SWP
Pile velocity (m/s)

. (*continued*).

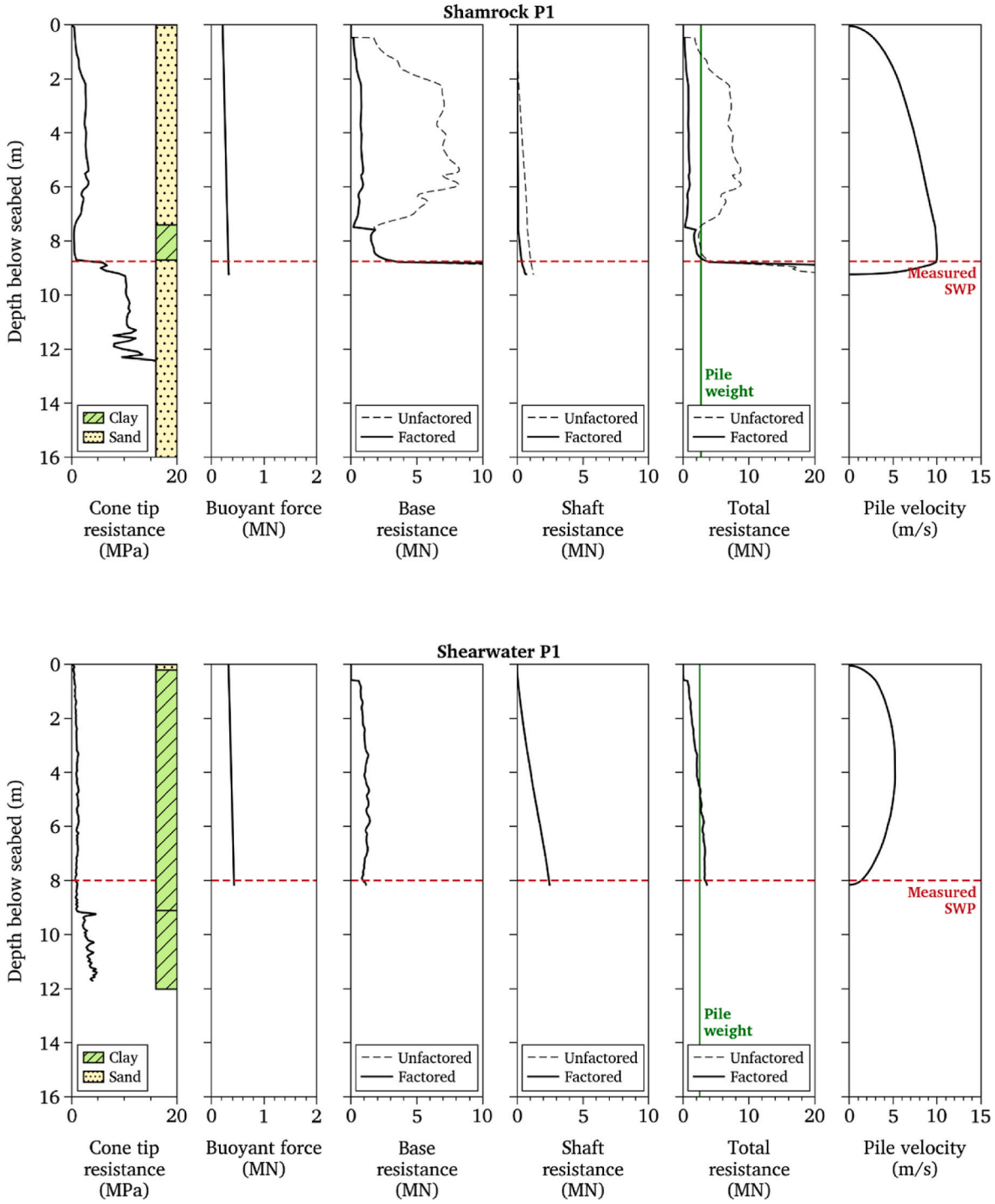
Shamrock P1
Depth below seabed (m)
Clay
Sand
Cone tip resistance (MPa)
Buoyant force (MN)
Unfactored
Factored
Base resistance (MN)
Shaft resistance (MN)
Pile weight
Total resistance (MN)
Measured SWP
Pile velocity (m/s)
Shearwater P1
Depth below seabed (m)
Clay
Sand
Cone tip resistance (MPa)
Buoyant force (MN)
Unfactored
Factored
Base resistance (MN)
Shaft resistance (MN)
Pile weight
Total resistance (MN)
Measured SWP
Pile velocity (m/s)

. (*continued*).

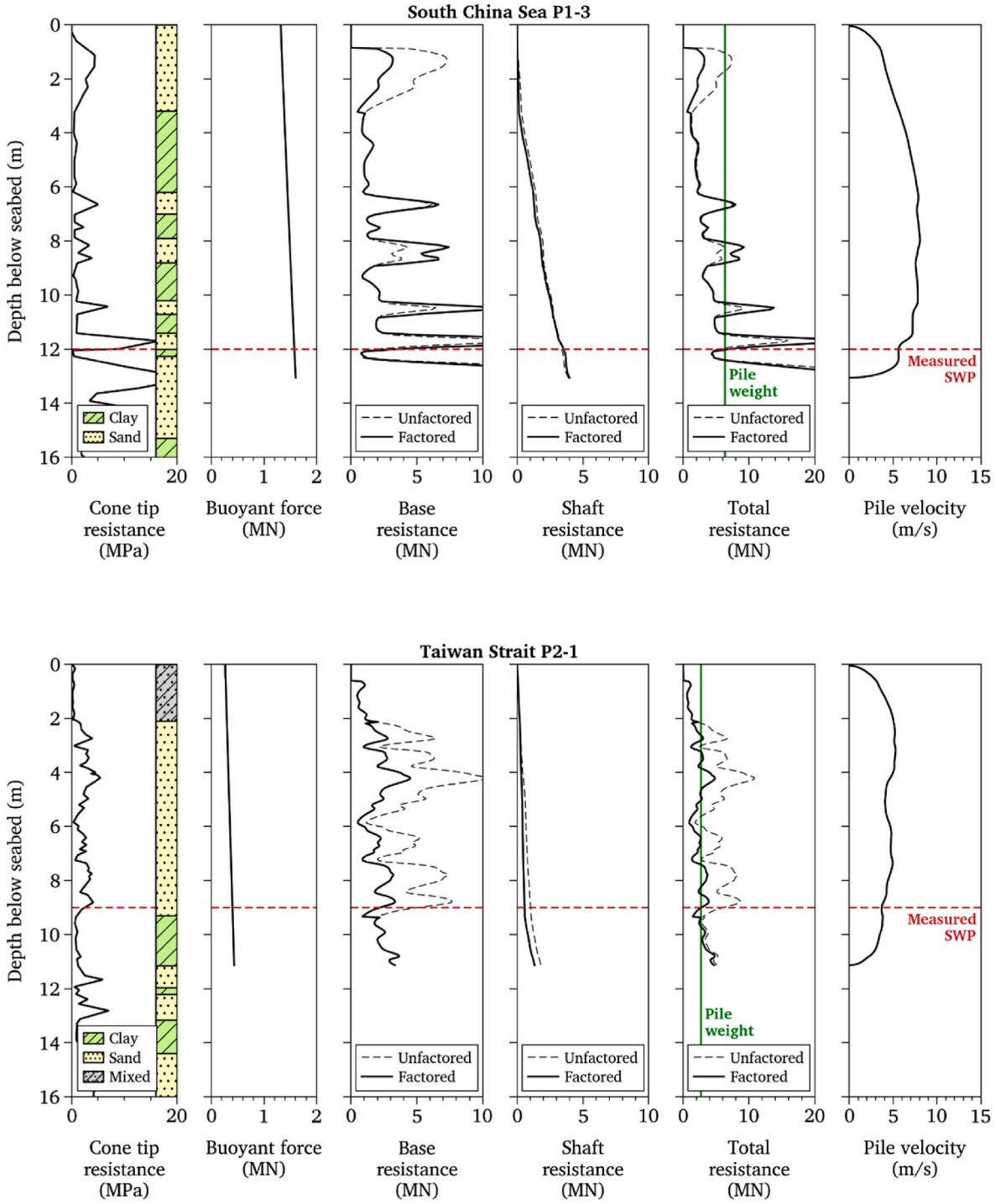
South China Sea P1-3
Depth below seabed (m)
Clay
Sand
Cone tip resistance (MPa)
Buoyant force (MN)
Unfactored
Factored
Base resistance (MN)
Shaft resistance (MN)
Pile weight
Total resistance (MN)
Measured SWP
Pile velocity (m/s)
Taiwan Strait P2-1
Mixed

. (*continued*).

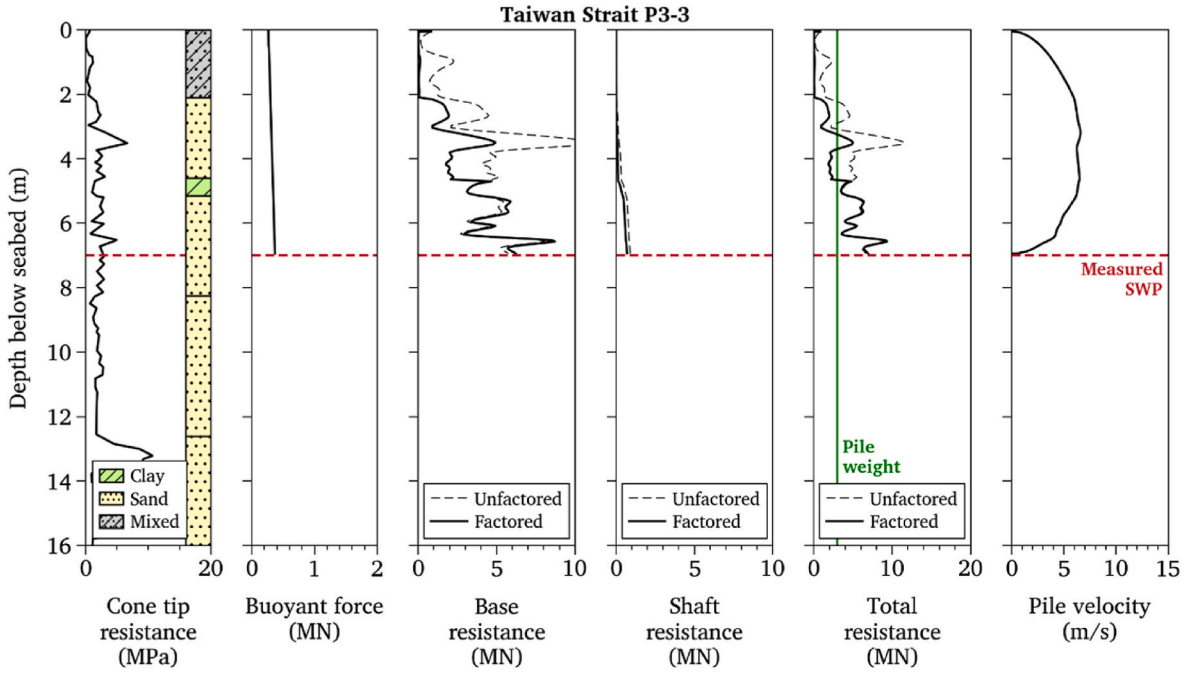

. (*continued*).

References

Albatal, A., Stark, N., Castellanos, B., 2020. Estimating in situ relative density and friction angle of nearshore sand from portable free-fall penetrometer tests. Can. Geotech. J. 57, 17–31. https://doi.org/10.1139/cgj-2018-0267.

Alm, T., Hamre, L., 2001. Soil model for pile driveability predictions based on CPT interpretations. In: Proceedings of the 15th International Conference on Soil Mechanics and Geotechnical Engineering. Presented at the International Conference on Soil Mechanics and Geotechnical Engineering. A. A. Balkema, Istanbul, Turkey, pp. 1297–1302.

API, 2011. Geotechnical and Foundation Design Considerations: ANSI/API Recommended Practice 2GEO, first ed. American Petroleum Institute, Washington DC, USA. ISO 19901-4:2003).

Argyroulis, K., Putteman, J., Gavin, K.G., Roubos, A.A., 2024. Pile driveability predictions of open ended tubular piles in sand using the unified method. In: Proceedings of the 18th European Conference on Soil Mechanics and Geotechnical Engineering (ECSMGE 24), pp. 2076–2080. Lisbon, Portugal.

Ayala, J., Fourie, A., Reid, D., 2023. A unified approach for the analysis of CPT partial drainage effects within a critical state soil mechanics framework in mine tailings. J. Geotech. Geoenviron. Eng. 149, 04023036. https://doi.org/10.1061/JGGEFK.GTENG-10915.

Bittar, E.M., Lehane, B.M., Liu, Z., Nadim, F., Lacasse, S., 2022. Application of the unified CPT method for driven piles to layered deposits. Géotech. Lett. 12, 251–257. https://doi.org/10.1680/jgele.22.00058.

Bolton, M.D., 1986. The strength and dilatancy of sands. Geotechnique 36, 65–78.

Bond, A.J., Jardine, R.J., 1991. Effects of installing displacement piles in a high OCR clay. Geotechnique 41, 341–363. https://doi.org/10.1680/geot.1991.41.3.341.

Boulanger, R.W., DeJong, J.T., 2018. Inverse filtering procedure to correct cone penetration data for thin-layer and transition effects. In: Proceedings of the 4th International Symposium on Cone Penetration Testing (CPT'18). Presented at the Cone Penetration Testing 2018. CRC Press, pp. 24–44.

Buckley, R., Chen, Y.M., Sheil, B., Suryasentana, S., Xu, D., Doherty, J., Randolph, M., 2023. Bayesian optimization for CPT-based prediction of impact pile drivability. J. Geotech. Geoenviron. Eng. 149, 04023100. https://doi.org/10.1061/JGGEFK.GTENG-11385.

Byrne, T., Gavin, K., Prendergast, L.J., Cachim, P., Doherty, P., Chenicheri Pulukul, S., 2018. Performance of CPT-based methods to assess monopile driveability in north sea sands. Ocean Eng 166, 76–91. https://doi.org/10.1016/j.oceaneng.2018.08.010.

Cathie, D., Jaeck, C., Ozsu, E., Raymackers, S., 2020. Insights into the driveability of large diameter piles. In: 4th International Symposium on Frontiers in Offshore Geotechnics (ISFOG 2020). Deep Foundations Institute, Austin, Texas, USA, pp. 757–766.

Cathie, D., Jardine, R., Silvano, R., Kontoe, S., Schroeder, F., 2023. Axial capacity ageing trends of large diameter tubular piles driven in sand. Soils Found. 63, 101401. https://doi.org/10.1016/j.sandf.2023.101401.

Cathie, D., Raymackers, S., Vergote, T., Haine, G., Saraiva, J., Burgraeve, A., 2024. End bearing of large diameter piles in sand during driving. In: Proceedings of the 43rd European Conference on Soil Mechanics and Geotechnical Engineering (ECSMGE24). Taylor & Francis, Lisbon, Portugal, pp. 2172–2177.

Chai, F., Liu, B., Xue, J., Duffy, K., 2025. Assessing direct CPT-based methods for predicting pile base resistance using coupled DEM-FDM simulations. Comput. Geotech. 183, 107230. https://doi.org/10.1016/j.compgeo.2025.107230.

Chow, F.C.-M., 1997. Investigations into the Behaviour of Displacement Pile for Offshore Foundations. Imperial College London, London, United Kingdom. Ph.D. Thesis).

Chow, S.H., Bienen, B., Randolph, M., 2020. Rapid penetration of spudcans in sand. In: Proceedings of the 4th International Symposium on Frontiers in Offshore Geotechnics (ISFOG). Deep Foundations Institute, USA, pp. 2238–2247.

Chow, S.H., Bienen, B., Randolph, M.F., 2018. Rapid penetration of piezocones in sand. Presented at the Cone Penetration Testing 2018. Taylor & Francis, Delft, The Netherlands, pp. 213–219.

Chow, S.H., Bienen, B., Randolph, M.F., Roy, A., 2022. Rapid soil-structure interactions in saturated sand. In: Proceedings of 20th International Conference on Soil Mechanics and Geotechnical Engineering. Presented at the 20th International Conference on Soil Mechanics and Geotechnical Engineering, Australian Geomechanics Society, pp. 2615–2620. Sydney, Australia.

Chow, S.H., O'Loughlin, C.D., Goh, C.L.V., McIlduff, R., White, D.J., Chow, F.C., 2023. A comparative field study of free-fall cone and sphere penetrometers in soft sediment. Ocean Eng 280, 114094. https://doi.org/10.1016/j.oceaneng.2023.114094.

Colreavy, C., O'Loughlin, C.D., Randolph, M.F., 2016. Estimating consolidation parameters from field piezoball tests. Geotechnique 66, 333–343. https://doi.org/10.1680/jgeot.15.P.106.

Danziger, F.A.B., Lunne, T., 2012. Rate effect on cone penetration test in sand. Geotech. Eng. J. SEAGS AGSSE 43 (4), 72–81.

Dayal, U., Allen, J.H., 1975. The effect of penetration rate on the strength of remolded clay and sand samples. Can. Geotech. J. 12, 336–348. https://doi.org/10.1139/t75-038.

DeJong, J.T., Randolph, M.F., 2012. Influence of partial consolidation during cone penetration on estimated soil behavior type and pore pressure dissipation measurements. J. Geotech. Geoenviron. Eng. 138, 777–788. https://doi.org/10.1061/(ASCE)GT.1943-5606.0000646.

DNV, 2019. Offshore Soil Mechanics and Geotechnical Engineering (No. DNV-RP-C212). Det Norske Veritas, Oslo, Norway.

Doherty, P., Gavin, K.G., 2011. Shaft capacity of open-ended piles in clay. J. Geotech. Geoenviron. Eng. 137, 1090–1102. https://doi.org/10.1061/(ASCE)GT.1943-5606.0000528.

Duffy, K.J., Gavin, K.G., Korff, M., de Lange, D.A., Roubos, A.A., 2024. Influence of installation method on the axial capacity of piles in very dense sand. J. Geotech. Geoenviron. Eng. 150. https://doi.org/10.1061/JGGEFK/GTENG-12026.

Dyson, A.P., Tolooiyan, A., Gavin, K.G., 2025. Evaluating clay stiffness effects on offshore pile running with the coupled eulerian lagrangian method. Comput. Geotech. 183, 107185. https://doi.org/10.1016/j.compgeo.2025.107185.

Gavin, K.G., Jardine, R.J., Karlsrud, K., Lehane, B.M., 2015. The effects of pile ageing on the shaft capacity of offshore piles in sand. In: Frontiers in Offshore Geotechnics III: Proceedings of the 3rd International Symposium on Frontiers in Offshore Geotechnics (ISFOG 2015). Taylor & Francis, Oslo, Norway, pp. 129–153.

Gavin, K.G., O'Kelly, B.C., 2007. Effect of friction fatigue on pile capacity in dense sand. J. Geotech. Geoenviron. Eng. 133, 63–71. https://doi.org/10.1061/(ASCE)1090-0241(2007)133:1(63.

Han, F., Ganju, E., Prezzi, M., Salgado, R., Zaheer, M., 2020. Axial resistance of open-ended pipe pile driven in gravelly sand. Geotechnique 70, 138–152. https://doi.org/10.1680/jgeot.18.P.117.

Holeyman, A.E., 1992. Keynote lecture: technology of pile dynamic testing. In: Proceedings of the 4th International Conference on the Application of Stress-Wave Theory to Piles. A. A. Balkema, The Hague, The Netherlands, pp. 195–215.

Hölscher, P., van Tol, A.F., Huy, N.Q., 2012. Rapid pile load tests in the geotechnical centrifuge. Soils found. Special Issue on IS-Kanazawa 9th International Conference on Testing and Design Methods for Deep Foundations 52, 1102–1117. https://doi.org/10.1016/j.sandf.2012.11.024.

Huy, N.Q., 2008. Rapid Load Testing of Piles in Sand: Effects of Loading Rate and Excess Pore Pressure (Phd Thesis). Delft University of Technology, Delft, The Netherlands.

Igoe, D.J.P., Gavin, K.G., O'Kelly, B.C., 2011. Shaft capacity of open-ended piles in sand. J. Geotech. Geoenviron. Eng. 137, 903–913. https://doi.org/10.1061/(ASCE)GT.1943-5606.0000511.

Jaeger, R.A., DeJong, J.T., Boulanger, R.W., Low, H.E., Randolph, M.F., 2010. Variable penetration rate CPT in an intermediate soil. In: Proceedings of the 2nd International Symposium on Cone Penetrometer Testing (CPT). Omnipress, Huntington Beach, CA, USA.

Jardine, R.J., 2023. The 6th ISSMGE McClelland lecture: time-dependent vertical bearing behaviour of shallow foundations and driven piles. In: Offshore Site Investigation Geotechnics 9th International Conference Proceedings. Society for Underwater Technology, pp. 25–78. https://doi.org/10.3723/GIRI9226. London, United Kingdom.

Jardine, R.J., Standing, J.R., Chow, F.C., 2006. Some observations of the effects of time on the capacity of piles driven in sand. Geotechnique 56, 227–244. https://doi.org/10.1680/geot.2006.56.4.227.

Jones, L., Rattley, M., Manceau, S., 2020. A CPT-based soil resistance to driving (SRD) method for offshore pile driveability analyses. In: Piling 2020: Proceedings of the Piling 2020 Conference. ICE Publishing, London, United Kingdom.

Kaltekis, K., Peuchen, J., 2022. A CPT-based method for estimation of undrained shear strength of sands and transitional soils. In: Cone Penetration Testing 2022. CRC Press, Bologna, Italy. https://doi.org/10.1201/9781003308829-68.

Karlsrud, K., 2012. Prediction of load-displacement Behaviour and Capacity of Axially Loaded Piles in Clay Based on Analyses and Interpretation of Pile Load Test Results (Phd Thesis). Norwegian University of Science and Technology, Trondheim, Norway.

Lehane, B.M., 2024. Ongoing development of applications of the cone penetration test in interpretation and design. In: Proceedings of the 7th International Conference on Geotechnical and Geophysical Site Characterization (ISC2024). Scipedia, Barcelona, Spain. https://doi.org/10.23967/isc.2024.305.

Lehane, B.M., Gavin, K.G., 2001. Base resistance of jacked pipe piles in sand. J. Geotech. Geoenviron. Eng. 127, 473–480. https://doi.org/10.1061/(ASCE)1090-0241(2001)127:6(473).

Lehane, B.M., Igoe, D.J.P., Gavin, K.G., Bittar, E.J., 2022a. Application of the unified CPT method to assess the driving resistance of pipe piles in sand. In: Proceedings of the 11th International Conference on Stress Wave Theory and Design and Testing Methods for Deep Foundations (SW2022). Zenodo, Rotterdam, The Netherlands. https://doi.org/10.5281/zenodo.7148653.

Lehane, B.M., Lim, J.K., Carotenuto, P., Nadim, F., Lacasse, S., Jardine, R.J., van Dijk, B., 2017. Characteristics of unified databases for driven piles. In: Offshore Site Investigation Geotechnics 8th International Conference Proceedings. Presented at the 8th Offshore Site Investigation and Geotechnics International Conference 2017. Society for Underwater Technology, London, United Kingdom, pp. 162–194. https://doi.org/10.3723/OSIG17.162.

Lehane, B.M., Liu, Z., Bittar, E.J., Nadim, F., Lacasse, S., Bozorgzadeh, N., Jardine, R., Ballard, J.-C., Carotenuto, P., Gavin, K., Gilbert, R.B., Bergan-Haavik, J., Jeanjean, P., Morgan, N., 2022b. CPT-based axial capacity design method for driven piles in clay. J. Geotech. Geoenviron. Eng. 148, 04022069. https://doi.org/10.1061/(ASCE)GT.1943-5606.0002847.

Lehane, B.M., Liu, Z., Bittar, E.J., Nadim, F., Lacasse, S., Jardine, R.J., Carotenuto, P., Rattley, M., Jeanjean, P., Gavin, K.G., Gilbert, R., Bergan-Haavik, J., Morgan, N., 2020. A new "unified" CPT-based axial pile capacity design method for driven piles in sand. In: Proceedings of the 4th International Symposium on Frontiers in Offshore Geotechnics. Presented at the International Symposium on Frontiers in Offshore Geotechnics (ISFOG). Deep Foundations Institute, Austin, Texas, USA, pp. 462–477.

Lehane, B.M., O'Loughlin, C.D., Gaudin, C., Randolph, M.F., 2009. Rate effects on penetrometer resistance in kaolin. Geotechnique 59, 41–52. https://doi.org/10.1680/geot.2007.00072.

Lim, J.K., Lehane, B.M., 2014. Characterisation of the effects of time on the shaft friction of displacement piles in sand. Geotechnique 64, 476–485. https://doi.org/10.1680/geot.13.P.220.

Liyanapathirana, D.S., Deeks, A.J., Randolph, M.F., 1998. Numerical analysis of soil plug behaviour inside open-ended piles during driving. Int. J. Numer. Anal. Methods GeoMech. 22, 303–322. https://doi.org/10.1002/(SICI)1096-9853(199804)22:4<303::AID-NAG919>3.0.CO;2-P.

Lunne, T., Kvalstad, T., 1982. Analysis of full-scale measurements on gravity platforms. Final Report: Foundation Performance During Installation and Operation of North Sea Concrete Gravity Platforms. Norwegian Geotechnical Institute, Oslo, Norway.

Luo, L., Zhou, X., Zhou, Z., Wang, W., Zhang, X., Li, J., 2025. Optimising suction bucket foundation installation for offshore renewable energy infrastructure through field data on self-weight penetration. Renew. Energy 244, 122646. https://doi.org/10.1016/j.renene.2025.122646.

Maynard, A.W., Hamre, L., Butterworth, D., Davison, F., 2019. Improved pile installation predictions for monopiles. In: Proc. 10th International Conference on Stress Wave Theory and Testing Methods for Deep Foundations. Presented at the 10th International Conference on Stress Wave Theory and Testing Methods for Deep Foundations. ASTM International, San Diego, CA, USA. https://doi.org/10.1520/STP161120170164.

Ogawa, N., Ishihara, Y., Yokotobi, T., Kinoshita, S., Nagayama, T., Kitamura, A., Tagaya, K., 2009. Soil plug behavior of open-ended tubular pile during press-in. In: Proceedings of the 2nd IPA International Workshop in New Orleans. New Orleans, USA.

O'Loughlin, C.D., Richardson, M.D., Randolph, M.F., Gaudin, C., 2013. Penetration of dynamically installed anchors in clay. Geotechnique 63, 909–919. https://doi.org/10.1680/geot.11.P.137.

Overy, R., 2007. The use of ICP design methods for the foundations of nine platforms installed in the UK north sea. In: Proceedings of the 6th International Offshore Site Investigation and Geotechnics Conference: Confronting New Challenges and Sharing Knowledge. OnePetro, London, United Kingdom.

OWA, 2019. Suction installed caisson foundations for offshore wind: design guidelines. Offshore Wind Accelerator (OWA).

Perikleous, G., Stergiou, T., Hansen, J.Y., Meissl, S., 2023. Methodology for developing and evaluating an SRD method based on offshore wind monopile driving records. In: Proceedings of the 9th International SUT Offshore Site Investigation and Geotechnics Conference. Presented at the Offshore Site Investigation Geotechnics 9th International Conference, pp. 736–743. https://doi.org/10.3723/CNBH1219. OnePetro, London, United Kingdom.

Prendergast, L.J., Gandina, P., Gavin, K.G., 2020. Factors influencing the prediction of pile driveability using CPT-based approaches. Energies 13, 3128–3147. https://doi.org/10.3390/en13123128.

Puech, A., Foray, P., 2002. Refined model for interpreting shallow penetration CPTs in sands. In: Proc. 2002 Offshore Technology Conference. Presented at the Offshore Technology Conference. https://doi.org/10.4043/14275-MS. OnePetro, Houston, USA.

Randolph, M., Hope, S., 2004. Effect of cone velocity on cone resistance and excess pore pressures: effect of cone velocity on cone resistance and excess pore pressures. Proc. Osaka - Eng. Pract. Perform. Soft Depos. n/a 147–152.

Randolph, M.F., 1987. Modelling of the soil plug response during pile driving. In: Proceedings 9th Southeast Asian Geotechnical Conference. Bangkok, Thailand, pp. 6.1–6.14.

Randolph, M.F., Leong, E.C., Houlsby, G.T., 1991. One-dimensional analysis of soil plugs in pipe piles. Geotechnique 41, 587–598. https://doi.org/10.1680/geot.1991.41.4.587.

Randolph, M.F., Stanier, S.A., O'Loughlin, C.D., Chow, S.H., Bienen, B., Doherty, J.P., Mohr, H., Ragni, R., Schneider, M.A., White, D.J., 2018. Penetrometer equipment and testing techniques for offshore design of foundations, anchors and pipelines. In: Cone Penetration Testing 2018. CRC Press, Delft, The Netherlands, pp. 3–23.

Rimoy, S., Silva, M., Jardine, R., Yang, Z.X., Zhu, B.T., Tsuha, C.H.C., 2015. Field and model investigations into the influence of age on axial capacity of displacement piles in silica sands. Geotechnique 65, 576–589. https://doi.org/10.1680/geot.14.P.112.

Robertson, P.K.J., 2021. Evaluation of flow liquefaction and liquefied strength using the cone penetration test: an update. Can. Geotech. J. 59, 620–624. https://doi.org/10.1139/cgj-2020-0657.

Robertson, P.K.J., 2010. Soil behaviour type from the CPT: an update. Presented at the 2nd International Symposium on Cone Penetration Testing, Huntington Beach, CA, USA.

Robinson, S., Brown, M.J., 2013. Rate effects at varying strain levels in fine grained soils. Presented at the Proceedings of the 18th International Conference on Soil Mechanics and Geotechnical Engineering (ICSMGE), ISSMGE, Paris, France, pp. 263–266.

Roy, A., Chow, S.H., Randolph, M.F., O'Loughlin, C.D., 2022. Consolidation effects on uplift capacity of shallow horizontal plate anchors in dilating sand. Geotechnique 72, 957–973. https://doi.org/10.1680/jgeot.20.P.117.

Scarfone, R., Schroeder, F.C., Silvano, R., Cathie, D., Jardine, R.J., 2023. Divergence between CPT based method predictions for the axial capacities of large offshore piles driven in sand. In: Offshore Site Investigation Geotechnics 9th International Conference Proceedings. Society for Underwater Technology, pp. 986–993. London, United Kingdom.

Schneider, J.A., Harmon, I.A., 2010. Analyzing drivability of open ended piles in very dense sands. DFI J. J. Deep Found. Inst. 4, 32–44. https://doi.org/10.1179/dfi.2010.003.

Semple, R.M., Gemeinhardt, P.J., 1981. Stress history approach to analysis of soil resistance to pile driving. In: Proc. 13th Offshore Technology Conference. Presented at the Offshore Technology Conference, pp. 165–183. https://doi.org/10.4043/3969-MS. OnePetro, Houston, USA.

Shonberg, A., Anusic, I., Harte, M., Schupp, J., Meissl, S., Liingaard, M.A., 2017. Comparison of self weight penetration prediction methods for large diameter monopiles in north sea soils. Presented at the Offshore Technology Conference. https://doi.org/10.4043/27763-MS. OnePetro, Houston, USA.

Silva, M.F., 2005. Numerical and Physical Models of Rate Effects in Soil Penetration (Phd Thesis). University of Cambridge, Cambridge, United Kingdom.

Smith, I.M., To, P., Wilson, S.M., 1986. Plugging of pipe piles. In: Proceedings of the 3rd International Conference on Numerical Methods in Offshore Piling. Nantes, France, pp. 53–73.

Stergiou, T., Perikleous, G., Meissl, S., 2023. MonoDrive: a novel SRD methodology for offshore wind monopile foundations developed based on an extensive driveability database. Offshore site investig. In: Geotech. 9th Int. Conf. Proceeding, pp. 744–748. https://doi.org/10.3723/CBWP3728.

Stevens, R.S., Wiltsie, E.A., Turton, T.H., 1982. Evaluating drivability for hard clay, very dense sand, and rock. In: Proc. 14th Offshore Technology Conference. Presented at the 14th Offshore Technology Conference, pp. 465–483. https://doi.org/10.4043/4205-MS. OnePetro, Houston, USA.

Sun, L., Jia, T., Yan, S., Guo, W., Ren, Y., Lei, Z., 2016. Prediction of pile running during the driving process of large diameter pipe piles. Ocean Eng 128, 48–57. https://doi.org/10.1016/j.oceaneng.2016.10.023.

Sun, L., Shi, J., Zhang, Y., Feng, X., Tian, Y., Wang, R., 2022. Analytical method for predicting pile running during driving. Appl. Ocean Res. 125, 103234. https://doi.org/10.1016/j.apor.2022.103234.

Suzuki, Y., 2015. Investigation and Interpretation of Cone Penetration Rate Effects (Phd Thesis). University of Western Australia, Perth, Australia.

Thijssen, R., Roelen, S., 2024. Prediction of pile run during pile driving - analytical model and field observations. Presented at the Offshore Technology Conference. https://doi.org/10.4043/35471-MS. OnePetro, Houston, USA.

Tian, Y., Cassidy, M.J., Zhao, H., 2022. Pile running problem and large deformation modelling. In: Proceedings of the 20th International Conference on Soil Mechanics and Geotechnical Engineering. Australian Geomechanics Society, Sydney, Australia.

Toolan, F.E., Fox, D.A., 1977. Geotechnical planning of piled foundations for offshore platforms. Proc. Inst. Civ. Eng. 62, 221–244. https://doi.org/10.1680/iicep.1977.3224.

White, D.J., 2002. An Investigation into the Behaviour of pressed-in Piles (Ph.D. Thesis). University of Cambridge, Cambridge, United Kingdom.

White, D.J., Lehane, B.M., 2004. Friction fatigue on displacement piles in sand. Geotechnique 54, 645–658. https://doi.org/10.1680/geot.2004.54.10.645.

White, D.J., O'Loughlin, C.D., Stark, N., Chow, S.H., 2018. Free fall penetrometer tests in sand: determining the equivalent static resistance. Presented at the Cone Penetration Testing 2018. CRC Press, Delft, The Netherlands, pp. 695–701.

Zhu, H., Randolph, M.F., 2011. Numerical analysis of a cylinder moving through rate-dependent undrained soil. Ocean Eng., Offshore Geotechnics 38, 943–953. https://doi.org/10.1016/j.oceaneng.2010.08.005.